*Transactions of the Royal Society of Edinburgh: Earth Sciences,* **94**, 503–521, 2004 (for 2003)

# Experimental taphonomy: silicification of plants in Yellowstone hot-spring environments

Alan Channing and Dianne Edwards

ABSTRACT: During experiments conducted within the vent pool of Medusa Geyser, Norris Geyser Basin, Yellowstone National Park, USA, amorphous opaline silica (opal-A) was deposited on/within plant tissues within 30 days of immersion. Initially, deposition created inter/intra-cellular films which lined cell walls plus intercellular colloid suspensions (sols) of opal-A nano/microspheres. By 330 days, opal-A deposition created a robust external and internal matrix that stabilised tissues against collapse and replicated plant structure. Opal-A films increased to micron-order thicknesses and intracellular sols were created. Systematic variation of opal-A fabric between tissues comprising living/dead cells at the time of deposition indicate that cell function, architecture and shape influence fabric development. Heterogeneity of opal-A fabric within adjacent cells of similar structure/function indicates spatially/temporally fluctuating physicochemical conditions and the presence of intra-organic microenvironments. Early deposition of opal-A films suggests a period of low silica supersaturation and slow opal-A deposition. In contrast, intracellular sols suggest high levels of supersaturation, and rapid opal-A deposition. Shell-like microsphere growth suggests cyclic variation of silica supersaturation, and alternations between rapid and slower opal-A deposition. Microsphere growth to the upper limit of colloidal stability and colloidal crystal structures indicate prolonged sol stability, whilst floc-like microsphere networks indicate localised sol instability.

KEY WORDS: Chert, colloidal, *Eleocharis*, Medusa Geyser, microsphere, Norris Geyser Basin, opal-A, permineralisation, Rhynie, silica, sol, subfossil.

Silica associated with permineralised fossil plants greater than a few tens of thousands of years old will have been subject to a series of well-documented structural and morphological transformations associated with crystallisation (e.g. Herdianita *et al*. 2000; Lynne & Campbell 2003; Rodgers *et al*. 2003). These transformations are accompanied/driven by periods of silica dissolution and reprecipitation which redistribute the solid phase. The cross-cutting silica veining associated with many fossil sinter deposits indicates additionally that the ageing of silica within hydrothermally active areas is accompanied by multiple post-depositional phases of silica emplacement (e.g. Powell *et al*. 2000). These post-depositional processes mask and/or obliterate primary deposition fabrics (e.g. Herdianita *et al*. 2000; Lynne & Campbell 2003; Rodgers *et al*. 2003).

Taphonomy experiments conducted in active hot-spring environments provide a means of observing the timing, rate, extent and fabric development sequences associated with higher-plant silicification during the critical initial period of immersion in silica-precipitating spring-fluid. The present authors describe and discuss the results of experiments conducted in a high-temperature hot-spring environment, the vent pool of Medusa Geyser, Norris Geyser Basin, Yellowstone National Park, Wyoming, USA (Fig. 1). Such direct observations of the silicification process provide a counterpoint perspective to the hypothetical sequences of the process elucidated from fossil material (e.g. Leo & Barghoorn 1976; Scurfield & Segnit 1984). The results of two experiments, of 30 and 330 days in duration, respectively, which record the character of silica deposits and paths of fabric development are presented. Additional information is provided by subfossil plant material from vent pool and sinter apron environments of the Norris area.

## 1. Methods

Medusa is a sporadically active geyser located in the Back Basin area of the Norris Geyser Basin, Yellowstone National Park. It has a c. 3·5 m diameter circular vent pool and narrow (c. 5 m wide) laminated to brecciated sinter apron (Fig. 2a–c). During the period of experimentation, the geyser was characterised by cyclic upwelling of vent fluid and eruptions which gently flooded and overtopped the vent pool rim (Fig. 2b), and discharged to adjacent wetlands (Fig. 2c). During a 20-h period of observation during August 1999, 39 eruptions of c. 5–15 min duration occurred at an average interval of 31 min (maximum = 113 min, minimum = 14 min). The vent fluid had an alkali-chloride character and Si concentration of 338–348 mg/kg$^{-1}$. Fluid temperature was in the range c. 52–81 °C and recorded pH varied between 6·1 and 7·5. Saturation indices (SIs) for the dissolved silica concentrations mentioned above, modelled with the PHREEQC for Windows Version 1.5.12 computer program, indicate that waters entering the vent pool from depth (SI = 0·11–0·12 at 75 °C), cooling within the vent pool rim system (SI = 0·27–0·28 at 50 °C) and flowing across the sinter apron (SI = 0·46–0·47 at 25 °C) were all supersaturated with respect to amorphous opaline silica (opal-A), plus chalcedony and quartz.

Freshly collected plant material was secured in water-permeable, fine-mesh nylon bags. Specimens of *Eleocharis rostellata* were picked, with their roots intact, from wetlands adjacent to the Norris Geyser Basin. *Eleocharis rostellata* was selected as the focus for analysis and observation, since the species was readily silicified in the natural environment. It is an extremely common component of silicified plant litter in adjacent wetlands and occurs in wetter regions of the sinter apron of Medusa (Fig. 2b, c). In addition, the species closely

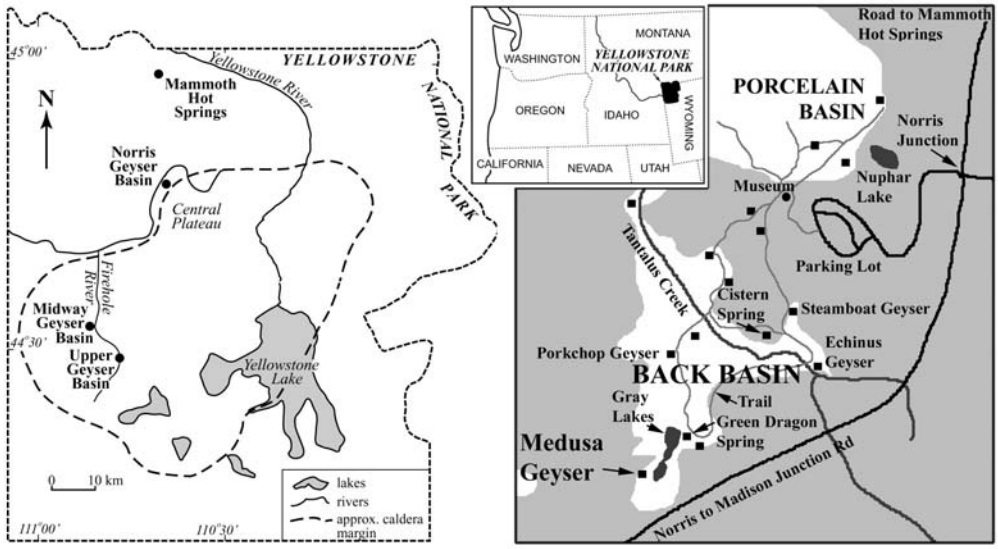


**Figure 1** Location maps of Yellowstone National Park and the Norris Geyser Basin showing the location of Medusa Geyser.

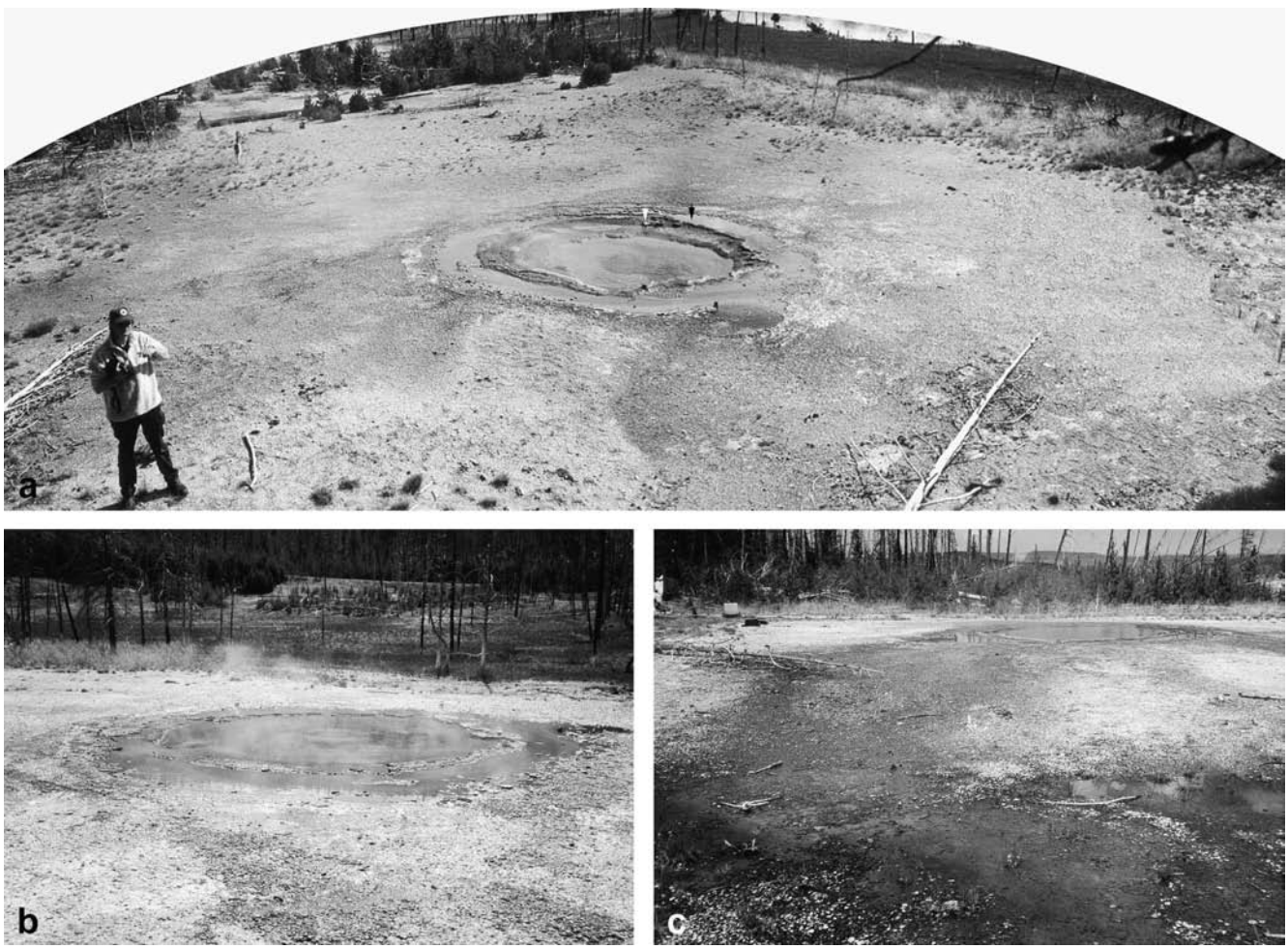


**Figure 2** Medusa Geyser, Norris Geyser Basin, Yellowstone National Park: (a) August 1999, sites of experimental material indicated by arrows. The vent fluid level is low following an eruption; (b) The pool during an eruptive event; (c) The vent fluid flowing across a sinter apron to the wetland margin (pool diameter = c. 3·5 m).

resembles Rhynie plants morphologically, being a rhizomatous, herbaceous perennial with naked stems. Anatomically, the species differs from Rhynie plants, possessing relatively large volumes of lignified cells and more extensive air spaces (see Fig. 3, sketch cell map). *Eleocharis flavescens* was used to provide supplementary data.

Experimental material was placed on a flat region of the geyser pool floor just within the pool rim system (arrows in Fig. 2a). The experimental material lay prostrate with the stems' long axes parallel to the pool floor during the experiment. This area was subject to periodic immersion by vent fluid (during eruption events and periods characterised by high vent

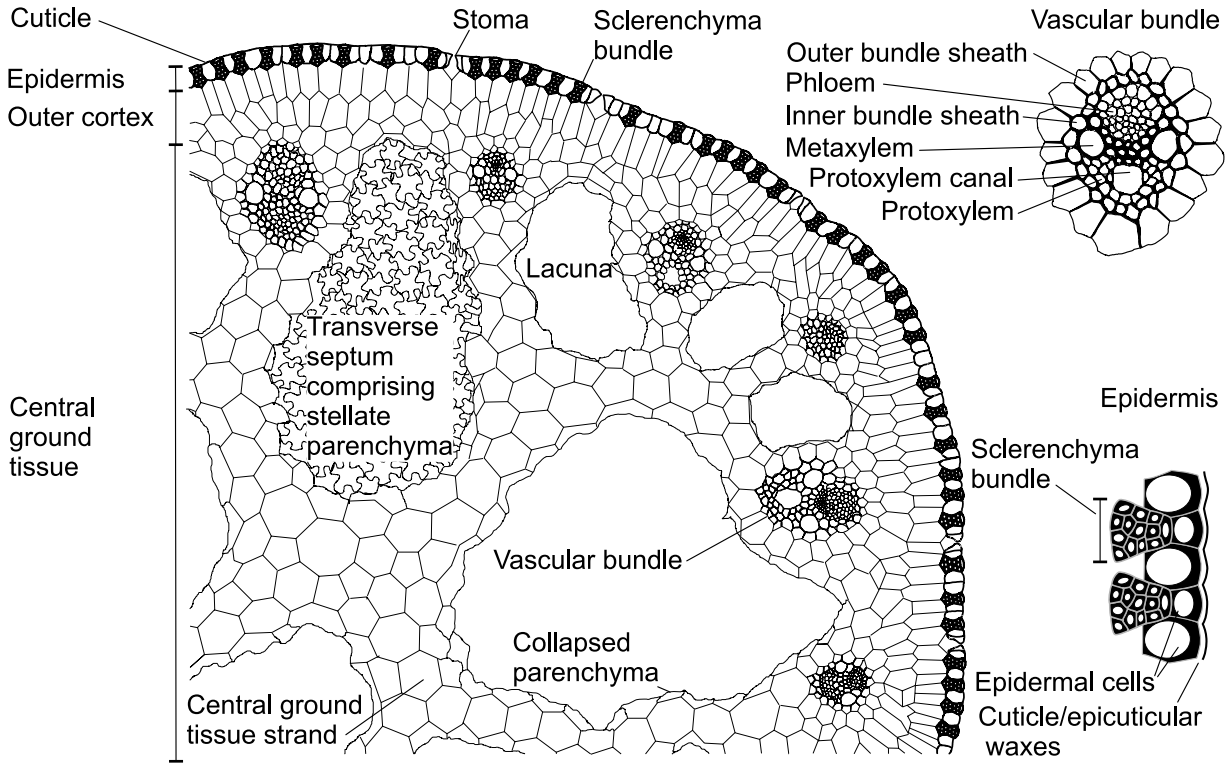


**Figure 3** Sketch cell map (transverse section) of the stem of *Eleocharis rostellata*.

fluid temperatures) and less frequent exposure during periods of low vent fluid level associated with cooling of the vent fluid and following eruption events which partially drained the vent pool.

Following 30 and 330 days immersion, samples were removed from the vent pool and fixed in the field by the addition of glutaraldehyde to vent fluid to give a 2% per volume final solution. Lightly silicified samples from the 30-day experiment were air dried or dehydrated by soaking in an alcohol series. Cut sections were mounted for scanning electron microscopy (SEM) and embedded in resin for transmission electron microscopy (TEM). More thoroughly silicified material from the 330-day experiment was fractured, mounted for SEM and sputter coated with gold/palladium.

Plant structure and silica deposits were observed with a Joel JEM1210 TEM and Cambridge Instruments S360 SEM. Oxford Instruments Energy Dispersive X-ray (EDX) spectrometers and Link ISIS analytical software fitted to the TEM/SEM were used to obtain EDX spot and area analyses, and Wavelength Dispersive X-ray (WDXM) and Energy Dispersive X-ray (EDXM) element maps. Mineral phases were further investigated by powder X-ray diffraction (XRD) with a Phillips PW1710 analytical X-ray diffractometer, with Cu Kα radiation.

Vent fluid temperature and pH data were gathered in the field using an Orion 230A temperature-calibrated pH/T meter. Real-time temperature data series were collected using Onset Computer Corporation, Stowaway XTI temperature loggers. Vent fluid elemental composition was investigated using atomic absorption spectroscopy (AAS) and inductively coupled plasma-mass spectrometry (ICPMS).

## 2. Results

### 2.1. Evidence of opal-A deposition

The TEM imaging and element analysis of 30-day material and the SEM imaging and element analysis of 330-day material investigated submicron- to micron-scale mineral deposits on and within stems.

**2.1.1. XRD, WDXM and EDX analysis of silica deposits.** The EDX analyses of 30-day material (Fig. 4a–d) indicated that electron-dense spheres, and opaque black films and lenses visible with TEM, comprised predominantly silicon and oxygen. Lesser amounts of calcium, iron and chlorine were also recorded (Fig. 4a–d). Silica deposition within cell walls (Fig. 4e, f) was less obvious, perhaps partly because of the size of initially polymerised mineral particles combined with the difficulty of observing particles against the organic matrix.

The XRD analysis of dried and powdered 330-day stem sections produced a broad diffraction band between 20° and 25°2θ indicative of X-ray amorphous opal-A. However, the peak count intensities of the diffraction band were shifted relative to the normal c. 4 Å (c. 25°2θ) peak of opal-A (Fig. 4g). The shift, broad peak width and extremely low count intensities obtained are most likely a reflection of the young age of the opal-A plus the incorporation of some organic material into the XRD powder sample.

The WDXM silicon distribution maps showed opal-A deposition within cell lumina, intercellular air spaces and within cell walls (Fig. 4h, i). The WDXM silicon maps and EDX spot analyses often produced similar count densities, count rates and similar Si spectra peak heights in both cell wall regions and intracellular particle aggregates, suggesting comparable silica concentrations. Silicon counts recorded whilst WDXM mapping 330-day material at 5 nA probe current were generally in the region of c. 5–8000 counts per 10 s, compared with the c. 200 counts per 10 s recorded after 30 days.

**2.1.2. Opal-A deposition on external surfaces.** Little opal-A was visible encrusting the surface of material following 30 days immersion. By 330 days, the external surfaces of air-dried stems were variably coated with powdery to knobby aggregates of opal-A microspheres (spherical particles of between 100 nm and 100 μm in diameter) and opal-A laminae of variable thickness and lateral extent (e.g. Figs 6a & 10b). The microstructure of external opal-A deposits was relatively

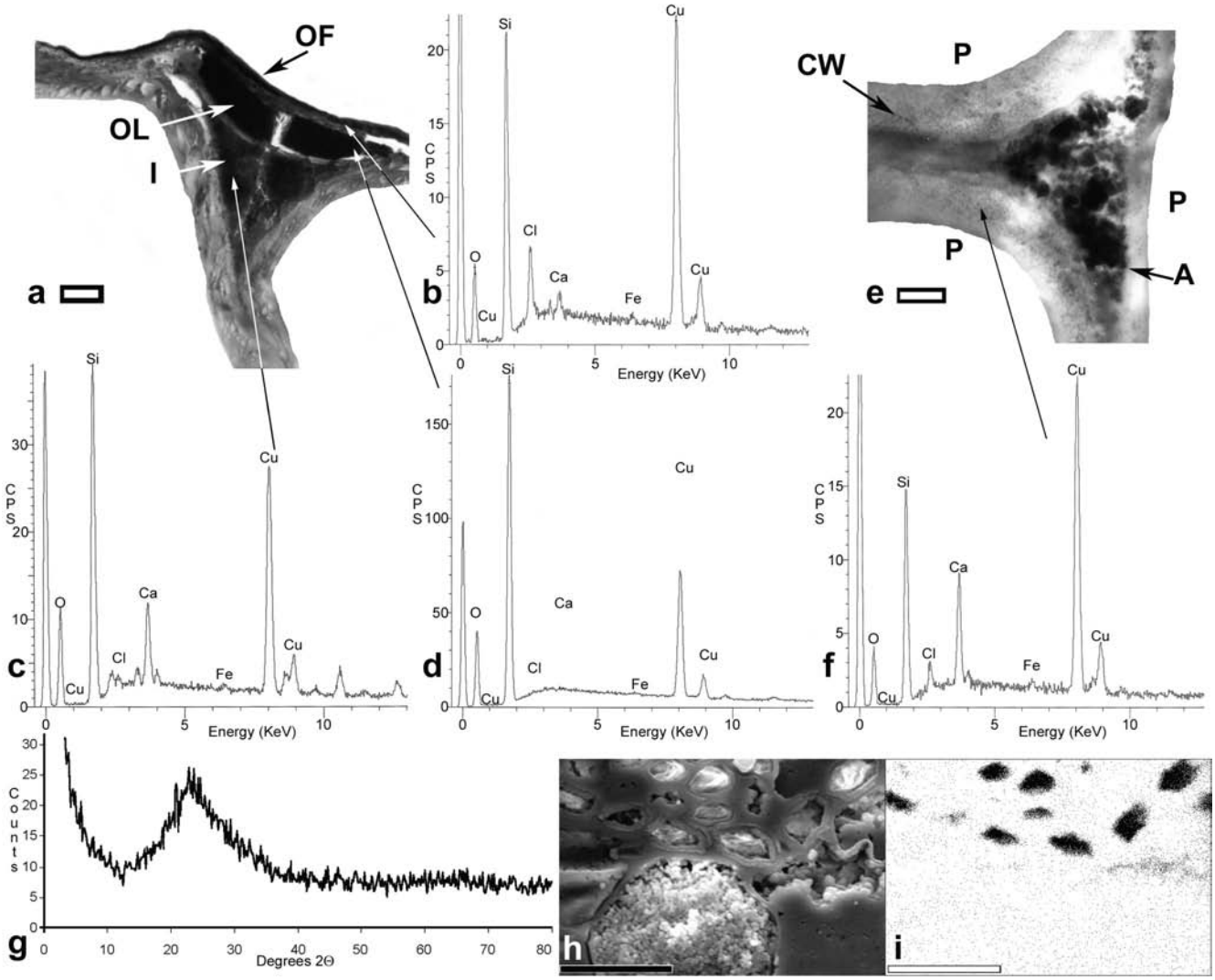


**Figure 4** X-ray analyses and photomicrographs of opal-A deposition within stems of *Eleocharis rostellata*: (a) Transmission electron microscopy (TEM) photomicrograph of intercellular and intracellular opal-A deposition within the central ground tissue of 30-day material (scale bar = 1 μm). Opal-A film (OF) lines the outer cell wall surface of a collapsed lacuna-lining parenchyma cell. The cell contains a fractured, electron-dense lens of opal-A (OL). The triangular intercellular region (I) between the parenchyma cell and two adjacent lightly lignified strand cells contains electron-dense regions of highly coalesced or cemented opal-A microspheres; (b–d) Energy dispersive X-ray (EDX) analyses of (b) lacuna-lining film, (c) opal-A within the intercellular space created by middle lamella degradation and (d) an intracellular lens in a collapsed lacuna-lining parenchyma cell; (e) A TEM photomicrograph of a triangular (T.S.) intercellular region between three adjacent parenchyma cells (P) of the outer cortex (30-day material) (scale bar = 200 nm). The intercellular region contains electron dense opal-A microsphere aggregates (A). Cell walls (e.g. CW) have a speckled appearance created by electron-dense regions tens of nanometres in scale; (f) An EDX analysis of a cell wall; (g) X-ray diffraction spectra illustrating the X-ray amorphous structure of permineralising opal-A; (h) A SEM photomicrograph of a region of silicified cells (330-day material) (scale bar = 20 μm). See Figure 7c–e for a detailed description; (i) Energy dispersive X-ray map (EDXM) of silica distribution within the stem region illustrated in (h); white regions = high numbers of silica counts (scale bar = 20 μm).

dense, compact and massive compared with intracellular deposits (e.g. Fig. 6a), and opal-A immediately adjacent to the cuticle/epidermis appeared to be structurally in continuity with the underlying organic substrate (Fig. 10b). Opal-A deposition on those surfaces of the stems which faced upwards during silicification reached up to c. 250 μm, whilst deposition on lower surfaces was negligible (e.g. Fig. 6a). Lenticular cavities formed between collapsed regions of the epidermal surface and the encrusting opal-A (Fig. 6a).

**2.1.3. Sites and fabrics of intercellular opal-A deposition.** The most common sites of opal-A deposition in 30-day material were the intercellular regions of the outer cortex (Figs 4e & 5a), central ground tissue (Fig. 4a), and also between parenchymatous cells of the outer bundle sheath and fibres of the inner bundle sheath (Fig. 5b). In compact tissues, homogeneous intercellular opal-A deposits occurred at the triangular (in T. S.) junctions of groups of three cells and in spaces created by degradation of the middle lamella (Fig. 4a). These regions often contained nanospheres (spherical particles with diameters of up to c. 100 nm) and nanosphere aggregates (Figs 4e, 5b). Within the larger lacunae of the central ground tissue, the outer walls of parenchymatous cells lining the lacunae were coated with opaque, relatively continuous opal-A films up to c. 200 nm thick (e.g. Fig. 4a).

Following 330 days, cell-encrusting films or microsphere aggregates lined the large (Fig. 6b, c) and small intercellular air spaces (Fig. 6e, f) of the inner and outer cortex. The surfaces of parenchymatous cells of the outer cortex and transverse septa were coarsely granular. Opal-A microspheres protruding from the surface were 2–300 nm in diameter (Fig. 6d). The outer

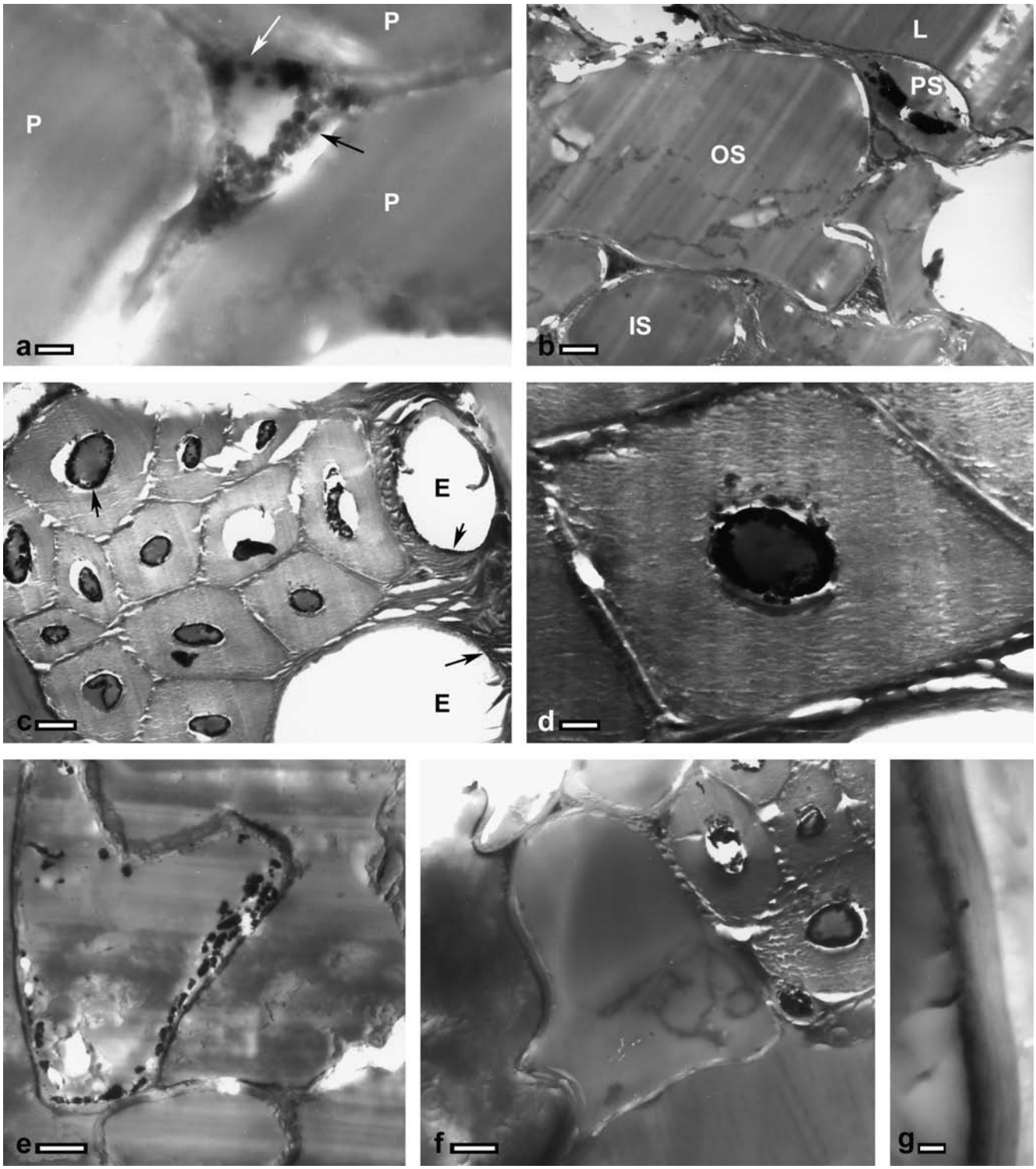


**Figure 5** Transmission electron microscopy (TEM) photomicrographs of opal-A deposition within *Eleocharis rostellata* stems following 30 days of immersion: (a) The triangular (T.S.) intercellular space between three parenchymatous cells (P) of the outer cortex. Opal-A microspheres form electron-dense areas of c. 100 nm in diameter (arrows) (scale bar = 200 nm); (b) A fibre of the inner vascular bundle sheath (IS), lightly lignified parenchymatous cells of the outer vascular bundle sheath (OS) and parenchymatous cell (PS) lining the lacuna (L). Opal-A does not appear in intracellular positions within the sheaths, but is present within the collapsed lacuna lining parenchyma. Dark-grey triangles at interstices of cells mark areas of intercellular opal-A deposition (scale bar = 2 μm); (c) Peripheral sclerenchyma bundle comprising 13 fibres and epidermal cells (E), all of which contain at least a partial lining of intracellular opal-A (arrows) (scale bar = 2 μm); (d) Fibre with a ~100–250-nm-thick opal-A film (black) encrusting the inner cell wall (scale bar = 500 nm); (e) Parenchymatous cell at the inner margin of the outer cortex containing blocky opal-A particles (scale bar = 2 μm); (f) A parenchymatous cell at the outer margin of the outer cortex (adjacent to peripheral sclerenchyma and epidermal cell) with an intracellular cell-wall lining film of opal-A (scale bar = 2 μm; (g) Enlarged region of (f) (scale bar = 200 nm).

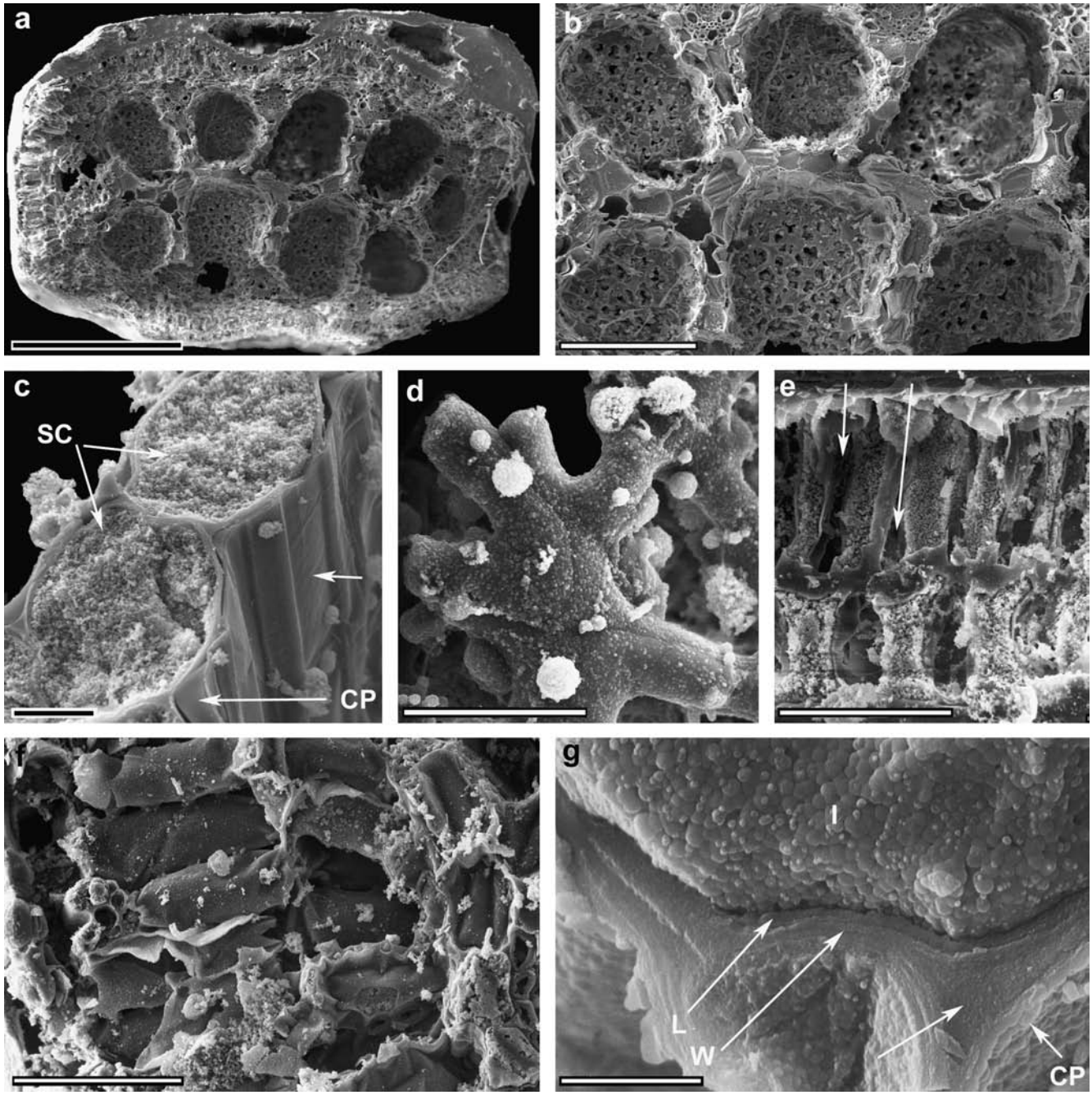


**Figure 6** Scanning electron microscopy (SEM) photomicrographs of opal-A deposition within *Eleocharis rostellata* stems following 330 days of immersion: (a) A stem (T.S.) and encrusting opal-A film (scale bar = 500 μm); (b) Central-ground-tissue, lightly lignified strand cells contain cell-filling opal-A microsphere aggregates. The empty cells probably result from plucking of cell-filling opal-A during specimen fracturing. The bases of the upper left and central lacunae contain open microsphere-aggregates (scale bar = 200 μm); (c) Lightly lignified ground tissue strand cells containing relatively open opal-A microsphere aggregates (SC) and collapsed parenchymatous cells with homogeneous blocks of intracellular opal-A (e.g. CP). Lacuna-facing surfaces of cells have a relatively smooth appearance (arrow) (scale bar = 20 μm); (d) Stellate parenchyma of transverse septa with granular coating of opal-A. Floc-like opal-A microsphere aggregates occupy intercellular positions (scale bar = 20 μm); (e) Cortical parenchyma (L.S.). Intercellular sites (e.g. arrows) remain free of voluminous microsphere networks, whilst open microsphere aggregates almost completely fill intracellular sites (scale bar = 50 μm); (f) Cortical parenchyma (T.S.). Cell surfaces have a granular opal-A coating (scale bar = 50 μm); (g) Intracellular opal-A deposition (I), cell wall (W) and wall-lining opal-A (L) within a large central ground tissue cell. Microsphere aggregate (I) is extremely dense and interparticle porosity essentially absent. Microsphere size distribution is relatively broad. The intracellular space within an adjacent collapsed lacuna-lining parenchyma cell (CP) has a wall-lining opal-A film with mammilate topography. The triangular (T.S.) region between the cells is filled with dense, internally homogeneous opal-A (arrow) (scale bar = 5 μm).

surfaces of the cells of the central ground tissue strands facing lacunae appeared to be less granular than other parenchymatous cells (Fig. 6c), and higher levels of magnification showed a moderately smooth surface with occasional hemispherical protrusions (Fig. 7e). Fractures across cell walls indicated that these intercellular opal-A films were similar in structure (homogeneous) and scale (c. 450–500 nm thick) to films lining cell-lumina (Fig. 7e).

The triangular (in T. S.) spaces at the junctions of strand cells (Fig. 6g) contained relatively dense opal-A deposited

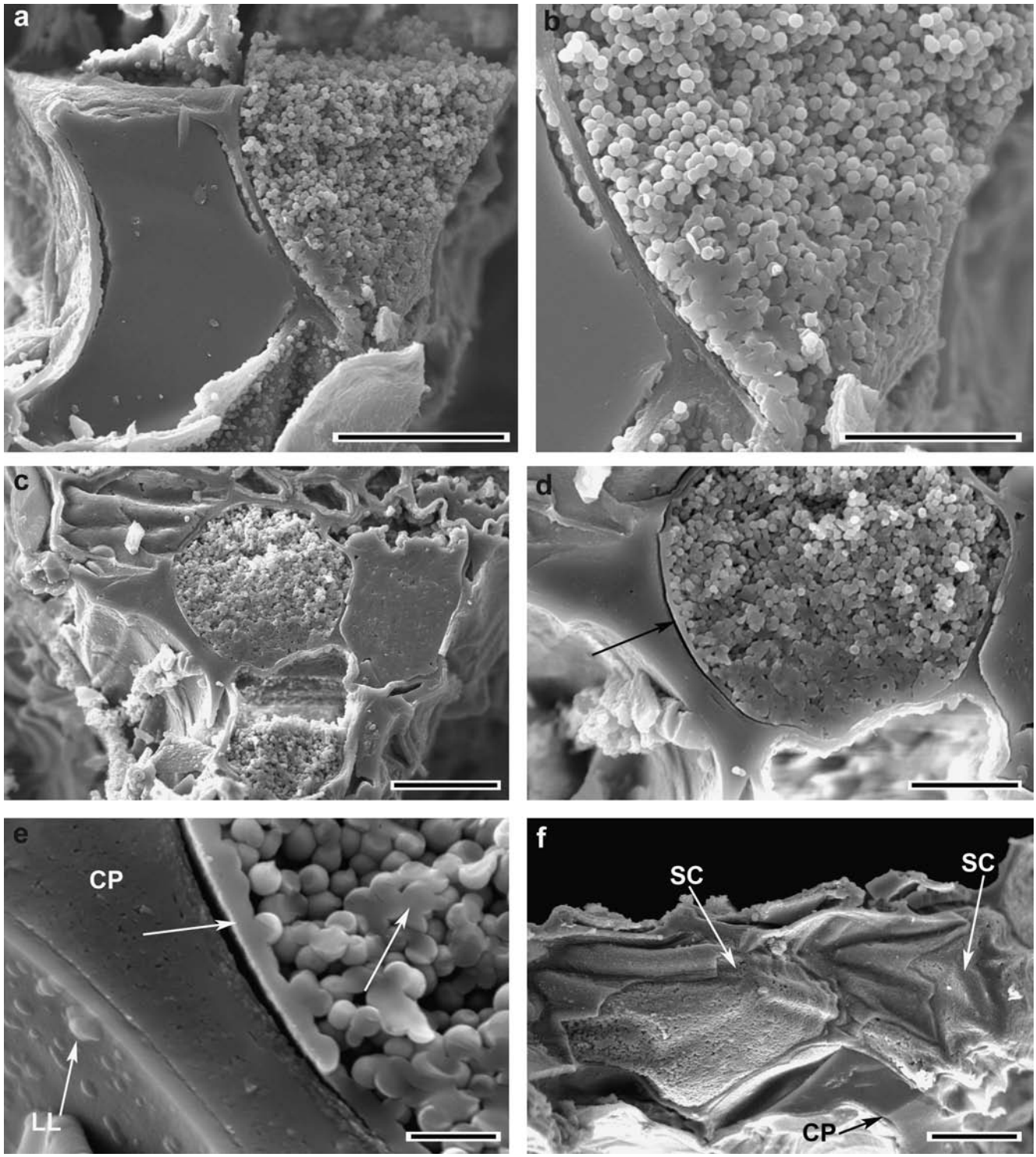


**Figure 7** Opal-A fabrics in 330-day material: (a) Contrasting cell fills in adjacent cells of similar function. The cell to the right contains a sediment of aggregated and coalesced opal-A microspheres with an essentially unimodal size distribution. The adjacent cell contains dense internally homogeneous opal-A; porosity is completely occluded except at the cell margins where hemispherical particles line probable remnant cell walls (scale bar = 20 μm); (b) Microsphere coalescence increases from the top of the sediment towards the base in the right hand cell (scale bar = 10 μm); (c) Three adjacent cells at the margin of the vascular bundle sheath and central ground tissue strand, each with different intracellular microsphere fabrics. The circular cell (T.S.) in the centre of image is almost completely filled by a network of aggregated microspheres. The cell below contains a population of microspheres of a similar size and size distribution which only partially fill the cell. The microsphere sediment remains relatively open. The cell to the right is only partially filled but microsphere coalescence/cementation and occlusion of porosity is extremely high (scale bar = 20 μm); (d) Intracellular microsphere aggregate coalesces at the cell margin to create a film-like region (arrow). Discontinuity between intracellular opal-A and the adjacent material appears to indicate delamination from the adjacent cell wall, perhaps as cell walls, swollen during opal-A deposition, contracted on removal from an aquatic environment. Microsphere coalescence increases within the cell from the top towards the base. At the base of the cell, porosity is almost completely occluded (scale bar = 10 μm); (e) Opal-A filling a collapsed lacuna-lining cell (CP) has little remnant porosity. Wall lining opal-A and intracellular microspheres (arrows) appear internally homogeneous. Hemispherical protrusions are prominent features of the opal-A film lining the lacunae margin (LL) (scale bar = 2 μm); (f) Dense intracellular microsphere aggregates in large strand cells (SC) and internally homogeneous, conchoidal fracturing, intracellular opal-A within a collapsed cell lining the lacuna (CP) (scale bar = 20 μm).

within the degrading middle lamella. Within some vascular bundles, the area formerly occupied by the protoxylem contained widespread deposits comprising cell-wall lining, opal-A films (Fig. 8g), microsphere aggregates (Fig. 8a) and internally homogeneous opal-A masses with botryoidal surfaces (Fig. 8b). Triangular (in T. S.) and sheet-like opal-A deposition extended from these regions into intercellular positions between vessels of the metaxylem and fibres of the vascular bundle sheaths (Fig. 8c). The c. 250-nm-thick sheets between cells were bounded to either side by parallel sided voids (of similar thickness) which probably corresponded with the sites of the cells former primary walls or S1, S2 layers of the secondary walls (Fig. 8c).

**2.1.4. Opal-A deposition in cell walls.** Opal-A deposition within cell walls following 30 days was not obvious with TEM. Electron-dense nanospheres, comparable in size with those of intracellular and intercellular fabrics, were observed rarely in thickened cell walls, but were often of ambiguous provenance, possibly representing plucked particles (Fig. 5d). Thin cell walls of the outer cortical parenchyma often exhibited a speckled internal fabric comprising apparently spherical, aggregated to fibrous, electron-dense domains with diameters of tens of nanometers (Fig. 4e). An EDX spot analysis of regions of the cell wall confirmed the presence of silica, but at lower count rates than dense intercellular and intracellular opal-A deposits (Fig. 4e, f).

Difficulties in sectioning for TEM prevented direct observation of the ultrastructure of cell walls and sites of intra-cell-wall opal-A deposition in 330-day material. Instead, analytical techniques were utilised to assess the properties of cell walls relative to presumably pure opal-A in intracellular positions. The EDX spectra for thickened cell walls and opal-A microsphere aggregates within their lumina were essentially the same. The WDXM and EDXM silicon distribution maps both suggested that deposition of opal-A had occurred within the cell walls. Cell wall areas returned Si count intensities closely comparable with those of pure opal-A within cells (Fig. 4i). Fractured primary (and to some extent secondary) cell walls also provided some evidence of structural and mechanical similarities to intra- and intercellular opal-A deposits since they exhibited clean, conchoidal fracture surfaces (Fig. 9b).

**2.1.5. Sites and fabrics of intracellular opal-A deposition.** Intracellular opal-A deposition following 30 days was common in the fibres of the peripheral sclerenchyma bundles and shallow epidermal cells (Fig. 5c, d), the collapsed thin-walled parenchymatous cells which lined the margins of the lacunae (Fig. 4a) and parenchymatous cells adjacent to the lacunae at the inner edge of the outer cortex (Fig. 5e). Opal-A deposition was less common in the fibres of the vascular bundle sheaths (Fig. 5b) and those parenchymatous cells of the outer cortex situated away from the lacunae margin (Fig. 5f, g). Opal-A deposition was not observed within the vascular strands or the larger central strand cells of the central ground tissue (Fig. 4a).

Within cells, opal-A deposition was generally confined to the inner wall surface facing the cell lumen, and comprised incipient films (Fig. 5f, g), impersistent blocky to spherical microparticles (Fig. 5e) and c. 50–250-nm-thick opaque films which completely lined the lumina (Fig. 5c, d). Nanospheres visible at high ( × 10k) magnification were c. 100 nm in diameter (Fig. 5d). Within collapsed cells, particularly those which lined the central ground tissue lacunae, homogeneous opal-A masses c. 1 μm thick completely filled the intracellular space of the cells. These exhibited a shattered appearance, most likely created during TEM sectioning (Fig. 4a).

After 330 days, opal-A deposits had developed to some extent in all tissues and cell types of the stem. Considerable variation in the degree and style of opal-A deposition was visible in similar, even adjacent, cells with the same structure and function.

The intracellular spaces of large epidermal cells between bundles of fibres (Fig. 9a), the cortical parenchyma (Figs 6e, 9b, c) and the large cells of the parenchymatous central ground tissue strands (Figs 6c, 7a–f) were commonly filled with aggregates of submicron opal-A microspheres. Microsphere networks completely filled the intracellular space of many cells, but the network retained an open structure. The microspheres which formed these cell-filling deposits all appeared to be of a similar order of size. Individual cells exhibited variable degrees of space filling (e.g. Fig. 7a–e). Microsphere sediments (in this context, sediment is used to describe a concentration of microspheres produced by sedimentation, i.e. the settling of suspended microspheres or microsphere aggregates under the action of gravity) partially filled many cells, indicating which way up the specimen was during silicification (Fig. 7a–d). Within some large strand cells, microsphere aggregates with a botryoidal surface topography lined regions of cell wall above basal (filling the area of the cell nearest the vent floor during silicification) microsphere sediments (Fig. 9d).

The narrower lumina of fibres and the broad, shallow epidermal cells above the sclerenchyma bundles contained pipe-like or solid, cylindrical opal-A masses with a homogeneous internal structure (Fig. 9a). Fibres surrounding the vascular strand contained intracellular opal-A in the form of sparse, often isolated microspheres and wall-lining films (Fig. 8b, e–g). The pipe-like deposits were similar in morphology to those observed in the 30-day material, but the thickness of deposition had increased from c. 250 nm to c. 1 μm (Fig. 5c, d, f, 9a).

The smaller lumina of thinner-walled, partially collapsed cells which lined the lacunae often contained homogeneous opal-A masses (cell at the bottom of Fig. 7f), whilst others had only wall-lining films (cells towards top of Fig. 7f). Homogeneous masses also filled the lumina of some large strand cells (Fig. 7a, b). Cell lumina which were completely empty or only had lumen-lining opal-A may have resulted from the plucking of lumen-filling deposits during fracturing. The cell wall areas exposed in such cells were characterised by coarse opal-A microsphere aggregates and films with granular surface topography.

Vessels exhibited extremely variable degrees of opal-A deposition. Vascular bundles which retained a relatively intact protoxylem often had metaxylem vessels which were essentially devoid of opal-A (Fig. 8f, g). Specimens with degraded protoxylem were often accompanied by opal-A-filled metaxylem vessels, plus opal-A infilling of the region created by the collapse of the protoxylem (Fig. 8b). Within vascular bundles where the protoxylem was preserved, intracellular sites were variably filled with cell-wall-lining films, microsphere aggregates and dense homogeneous opal-A masses which filled the available intracellular space (Fig. 8e).

The cells of the phloem exhibited several opal-A fabrics comparable with those observed in the xylem. Where phloem cells had collapsed or were in the process of collapsing, microspheres occurred within intracellular spaces and films with botryoidal surfaces lined cell walls (upper right region of the phloem in Fig. 8b). However, cells generally retained their original shape; the centres of their cell lumina remained open and free of dense opal-A deposition (Fig. 8d). Comparison of the thickness of cell walls and cell-wall-lining deposits of silicified samples (c. 925–1025 nm including middle lamella in Fig. 8d) and non-silicified samples (c. 150–225 nm including middle lamella) indicated that parallel-sided, internally homogeneous opal-A films c. 775–800 nm thick lined the walls of cells.

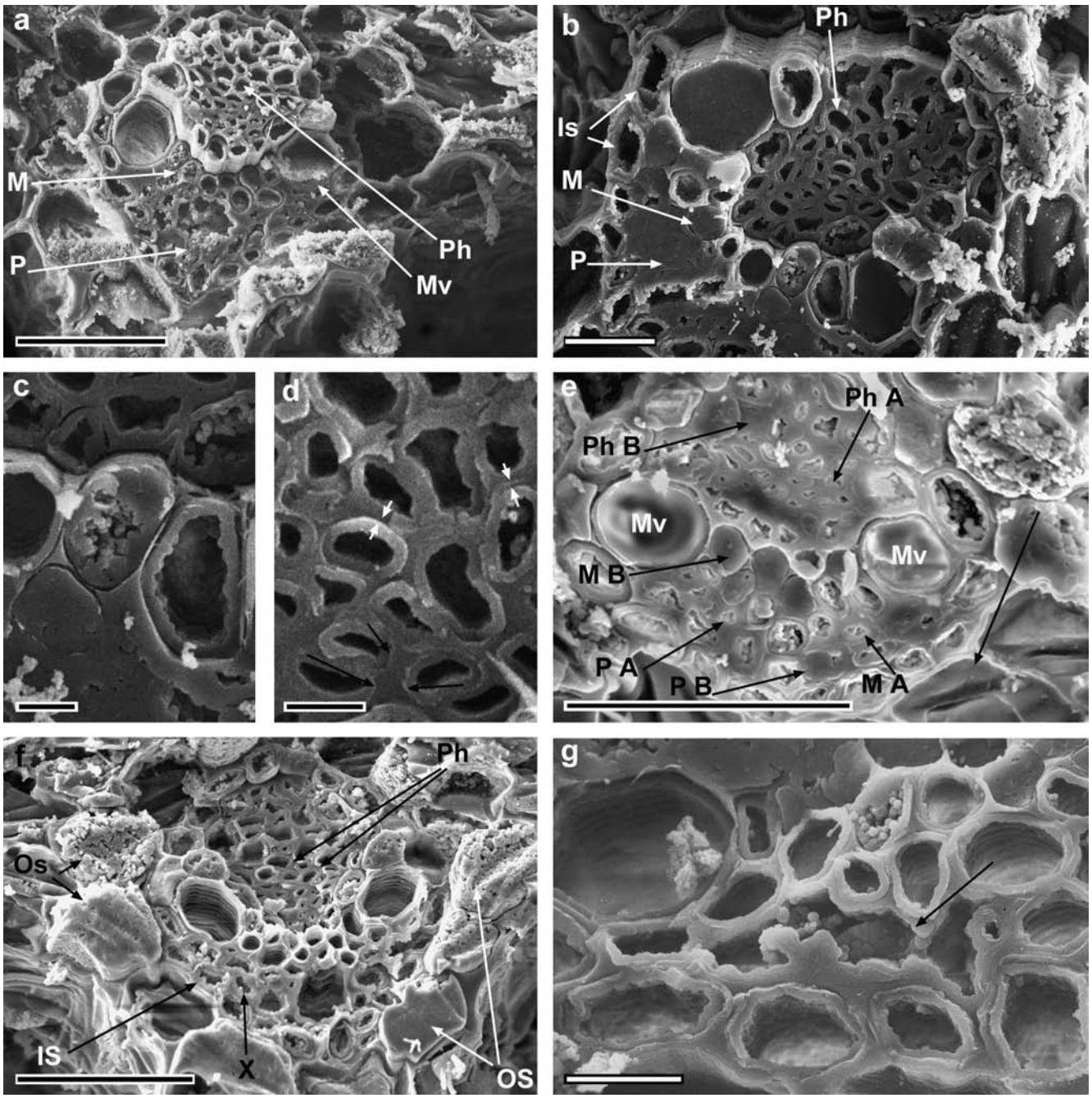


**Figure 8** Opal-A deposition following 330 days within vascular bundles: (a) Vascular bundle with a degraded region of protoxylem (P) and the cells of the metaxylem (M) containing space-filling opal-A-microsphere aggregates. Cells of the phloem (Ph) and metaxylem vessels (Mv) have wall-lining opal-A films (scale bar = 50 μm); (b) Vascular bundle with internally homogeneous opal-A almost completely filling the degraded protoxylem (P) and the cells of the metaxylem (M). Cells of the phloem (Ph) and inner bundle sheath (Is) contain wall-lining opal-A films (scale bar = 20 μm); (c) Enlarged view of the metaxylem of (b) (scale bar = 5 μm); Opal-A deposited in the degraded protoxylem appears to be in structural continuity with extremely thin 'blades' of material between adjacent metaxylem vessels and extends into the triangular (T.S.) junction between three cells (such positions are usually occupied in the living plant by the lignified, composite middle lamellae and primary wall; (d) Enlarged view of the phloem of (b) (scale bar = 5 μm); Parallel-sided intracellular opal-A films create the impression of secondarily thickened walls in the parenchymatous phloem. Areas between cell-wall-lining films (white arrows) may correspond to areas of cell wall. In other areas (between black arrows), the region between opal-A films appears too large to represent cell wall, perhaps indicating that cells separated/shrank and opal-A was deposited between them); (e) Vascular bundle with intact protoxylem. Thick, wall-lining opal-A films in the protoxylem (PA), metaxylem (MA) and phloem (PhA) appear to have developed into solid cylinders of internally homogeneous opal-A which completely fill the cells (PB, MB PhB). The large metaxylem vessels (Mv) have only wall-lining opal-A films (scale bar = 50 μm); (f) Vascular bundle with outer sheath (OS) cells containing microsphere aggregates and blocky internally homogeneous opal-A. Cells of the inner sheath (IS), phloem (Ph) and xylem (X) contain wall-lining films often associated with projecting microsphere aggregates (scale bar = 50 μm); (g) Metaxylem canal containing botryoidal/knobby opal-A microsphere aggregate (arrow) (scale bar = 10 μm).

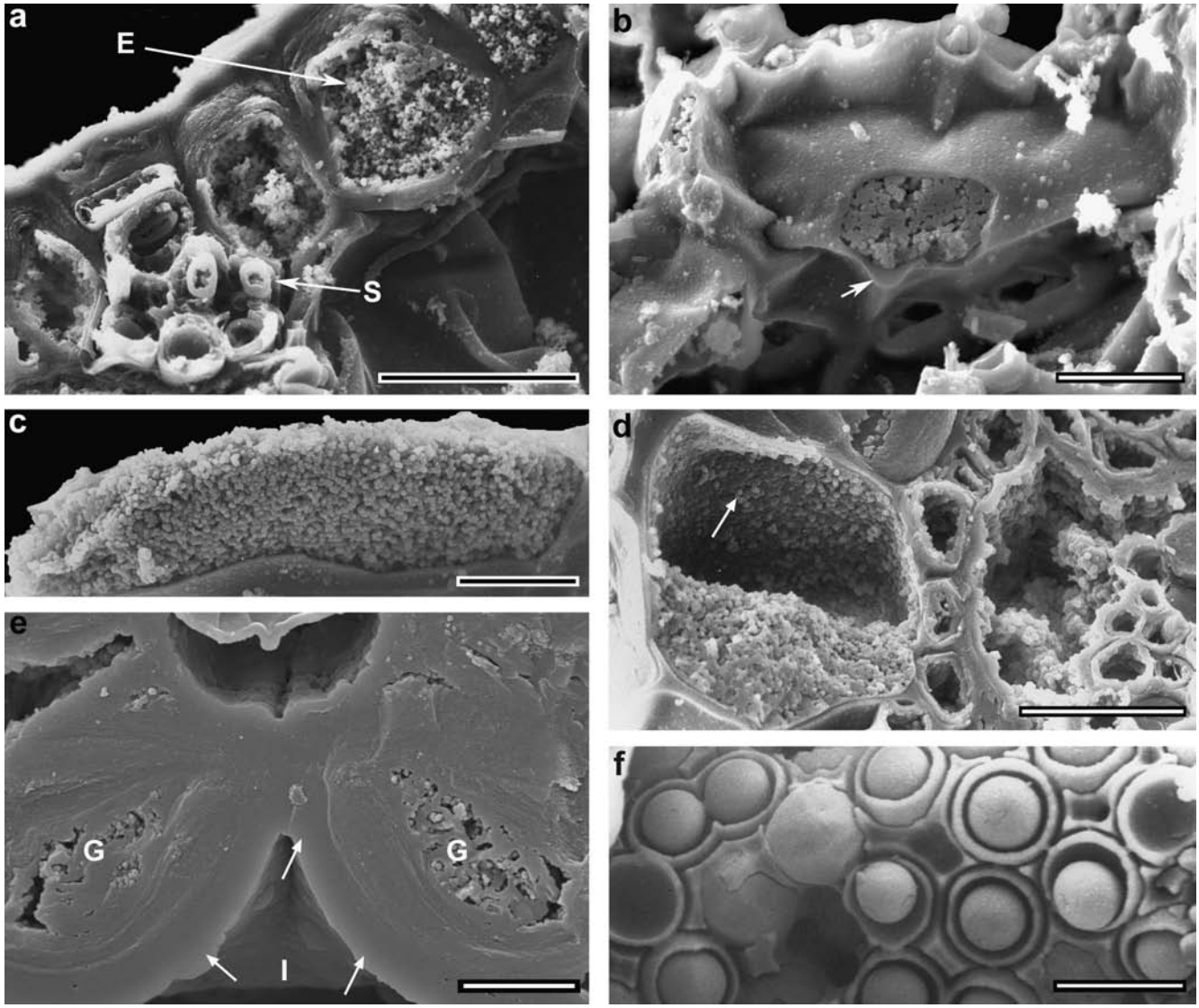


**Figure 9** Opal-A deposition following 330 days: (a) A large epidermal cell (E) containing open microsphere aggregate. The fibres of the sclerenchyma bundle (S) contain cylindrical films or rods of opal-A. The thick cell walls are partially degraded; gaps are present between the intracellular opal-A and the cell walls, and the bundles are beginning to disaggregate and separate from the adjacent epidermal cells (scale bars = 20 μm); (b) A partially collapsed parenchymatous cell of the outer cortex. The cell walls were coated with opal-A prior to their disintegration, but remnant cell wall material is not apparent within the opal-A coating (arrow). The cell contains a disordered, open network of opal-A microspheres (scale bar = 10 μm); (c) Three-dimensionally preserved cortical cell illustrating the creation of a three-dimensional, intracellular-network of coalesced and/or cemented opal-A microspheres. The open nature of the microsphere network suggests aggregation via colloidal processes whilst suspended in an aquatic medium (scale bar = 10 μm); (d) A cell containing a microsphere sediment that partially fills the cell. The 'roof' of the cell is coated with microspheres (arrow) which are of a similar size to those in the 'base' of the cell, suggesting that the microspheres were suspended as colloids in a stable sol that filled the cell immediately prior to sedimentation (scale bar = 20 μm); (e) Sunken stoma of a pine needle with dense opal-A deposition (arrows) extending from intracellular space (I) in the substomatal chamber between open guard cells (G) (scale bar = 10 μm); (f) Hydrofluoric acid etched intracellular opal-A, a network of opal-A cement surrounds opal-A microspheres with an internal structure comprising concentric spherical layers (scale bar = 2 μm).

## 2.2. Common opal-A fabrics

A number of commonly occurring, morphologically distinct opal-A fabrics developed during the 330-day period of this study. Common microfabrics included isolated microspheres, loose floc-like to dense coagulum-like or coalesced microsphere aggregates and sediments, and internally homogeneous films and masses.

**2.2.1. Opal-A nano-/microspheres.** Opal-A nanospheres and microspheres were the major component of opal-A deposits. Variations in the degree of sorting, aggregation, coalescence and cementation created a continuum series of opal-A microfabrics. Microsphere size ranged from that barely discernable with the SEM (hundreds of nanometres) to c. 1 μm. Microsphere diameters between 500 nm and 1000 nm were common (e.g. Figs 7b, d, 9c, 10e, f). Opal-A microsphere size distributions within individual intracellular spaces, a group of cells or a region of tissue often appeared to be relatively narrow. Individually discernable microspheres rarely, if ever, exceeded c. 1 μm, a size considered to be at the upper limit of colloidal particles (e.g. Iler 1979; Bergna 1994; Everett 1994). Fractured microspheres apparently possessed a homogeneous internal structure at the resolution available with SEM techniques (e.g. Fig. 7e); however, hydrofluoric-acid-etched subfossil material revealed an internal structure of concentric layers (Fig. 9f).

**2.2.2. Opal-A microsphere microfabrics.** Single cell lumina usually contained a number of distinct opal-A microfabrics

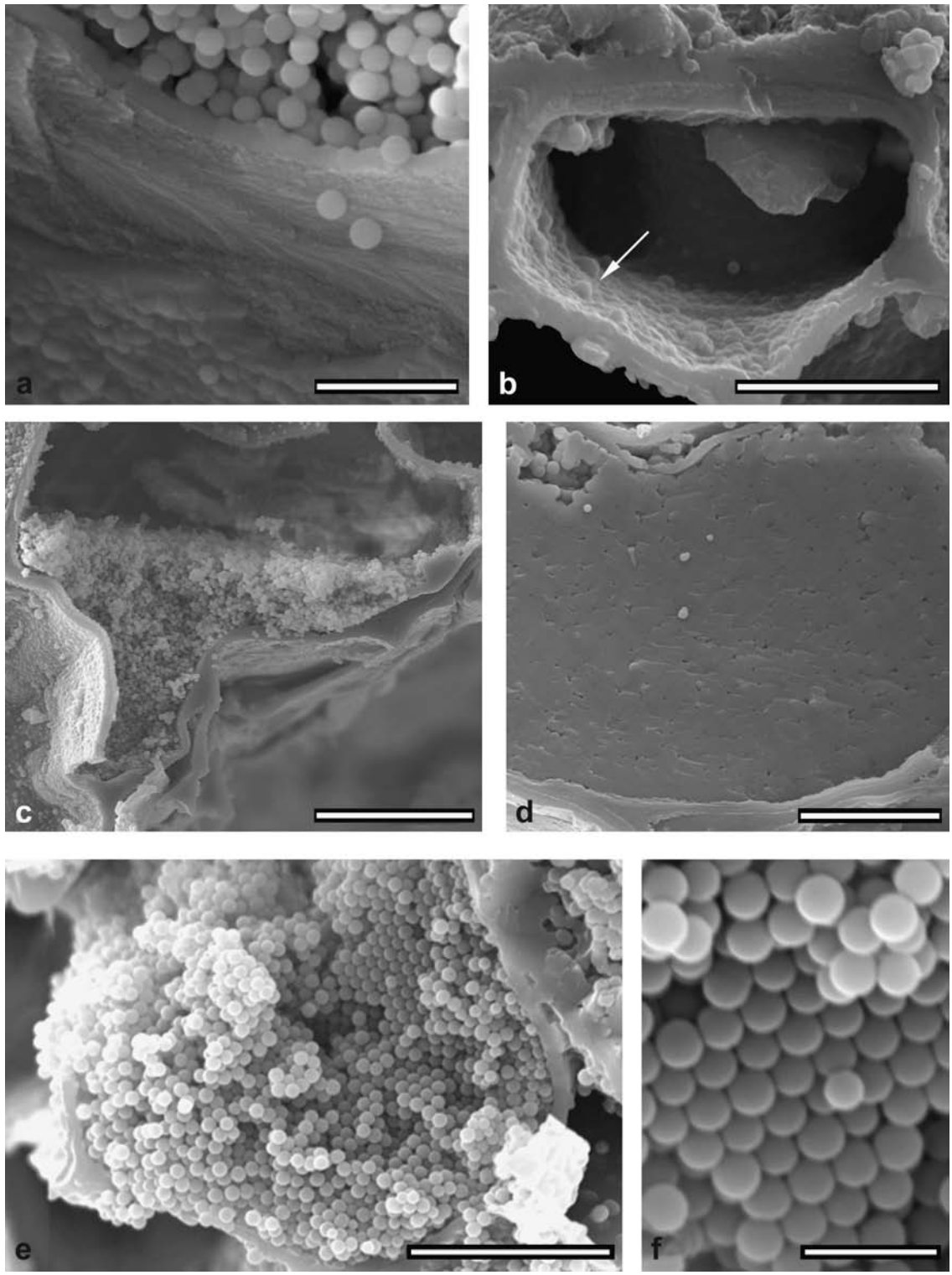


**Figure 10** Opal-A fabrics in cells of 330-day material: (a) Opal-A film deposition in inter- (mammilate surface, bottom left) and intracellular (film adjacent to microsphere aggregate) positions on either side of the lightly lignified wall of a central ground tissue strand cell (scale bar = 2 μm); (b) An epidermal cell of *Eleocharis flavescens*. The inner surface of the cell wall has a warty film of hemispherical opal-A particles (arrow). A small aggregate of microspheres at the outer margin of the cell forms a knobbly botryoidal projection into the cell space. The stem surface has an opal-A coating that appears to be in structural continuity with the underlying cuticle (scale bar = 10 μm); (c) A large, lightly lignified cell of the central ground tissue containing an open, poorly coalesced sediment of opal-A microspheres with a floc-like structure (scale bar = 20 μm); (d) Microsphere aggregate within a large cell of the central ground tissue illustrating a high degree of microsphere coalescence/cementation. Intracellular space is almost completely occluded (scale bar = 10 μm); (e) *Eleocharis flavescens*, parenchymatous cell of the outer cortex containing a microsphere sediment with an essentially unimodal size distribution. The sediment at the outer margin of the cell is disordered, partially aggregated and coalesced. At the inner cell margin, the microsphere sediment has domains of order (scale bar = 10 μm); (f) The microsphere sediment exhibits hexagonal close packing; the microspheres are not coalesced (scale bar = 2 μm).

which morphologically merged laterally and/or vertically into one another (e.g. Figs 7a–d, 9d). Internal cell wall regions were often characterised by individual or platy aggregates of microspheres, or an opal-A film with a granular surface texture, comparable with those observed on many external cell surfaces (e.g. Fig. 7e). The centres of cell lumina generally contained populations of microspheres exhibiting variable, but often systematically changing, degrees of sorting, packing, aggregation and coalescence (e.g. Fig. 7a–d).

**2.2.3. Cell-wall-lining opal-A microfabrics.** Intracellular cell wall surfaces were always observed to have wall-lining opal-A deposition. Within cells which lacked other intracellular opal-A deposits and those cells containing open microsphere networks, wall-lining films were generally of a similar morphology and thickness to deposits lining external wall surfaces (e.g. Fig. 10a, b). Hemispherical protrusions created a warty, lumina-facing fabric (e.g. Fig. 10b). Small aggregates of microspheres formed knobbly projections which were randomly distributed and orientated within lumina (Figs 7e, 10b). Within cells with a higher density of intracellular microspheres, these projections merged with intracellular microsphere aggregates (Fig. 7e). Fracture surfaces often intersected the presumed contact between these intracellular deposits and silicified cell walls. Where present, the surface of contact appeared planar parallel to the cell-wall surface (Fig. 9b). Transverse fracture sections commonly revealed the planar delamination of cell-wall lining deposits and adjacent areas of presumed cell wall (Fig. 7e). Other intracellular deposits merged imperceptibly with material in the region occupied in life by the cell wall (e.g. the intracellular deposit in the collapsed cell of Fig. 7e).

**2.2.4. Microsphere aggregates.** Microsphere aggregates, particularly those in intracellular sites, showed an obvious continuum of aggregation, coalescence and cementation states between isolate microspheres and dense indurated internally homogeneous masses (e.g. Fig. 7a, b). States within this continuum included:

- Open, floc-like microsphere aggregates with little or no microsphere coalescence (top surface of the microsphere aggregate within the righthand cell of Fig. 7a).
- Open microsphere aggregates with low numbers of microsphere contact points and/or low degree of microsphere coalescence (Fig. 10c).
- Less open, network-like microsphere aggregates with higher numbers of microspheres in close proximity because of crude close-packing and higher numbers of microsphere contact points, and a greater degree of coalescence (top of cell Fig. 7b).
- Dense microsphere aggregates, where the space between the microspheres is extremely reduced and often occluded, but where individual microspheres are discernible (base of the cell in Fig. 7b).
- Microsphere aggregates where individual microsphere margins were not visible, but occluded porosity indicates remnant interparticle voids (Fig. 10d).
- Homogeneous opal-A masses where intracellular and interparticle voids are essentially absent (left-hand cell of Fig. 7a).

Single cells were observed that exhibited only one microsphere fabric, but commonly, cells displayed a variety of fabrics. Systematic variations from open floc-like to dense microsphere aggregates were apparent in many cells. In most instances, interparticle porosity is interpreted to have decreased toward the base of cells and microsphere coalescence increased (e.g. Fig. 7a–d). An additional fabric was observed within the epidermal region of *E. flavescens* that comprised microspheres with a unimodal size distribution and nearly perfect hexagonal close packing (Fig. 10e, f).

## 3. Silica sources and pathways

Water rising into and flowing from the vent pool of Medusa Geyser cools from reservoir temperatures, commonly c. 360°C at Norris Geyser Basin (Kharaka *et al.* 2000), to below 80°C, and rapidly becomes supersaturated with respect to amorphous silica (opal-A). Supersaturation of vent fluid prior to permeation of plant material is illustrated by opal-A deposition onto the external surfaces of experimental material. Supersaturation of permineralising fluids prior to contact with the plant's organic frame make hot-spring environments and hot-spring silicification fundamentally different to silicification in the silica-undersaturated, waterlogged, volcanoclastic sediments considered by Leo & Barghoorn (1976). The scouring and orientated attachment of monosilicic acid from groundwater to cell-wall biomolecules and the local increase of silica concentrations to above the point of saturation, which the above authors considered caused polymerisation, is not required.

Following 30 days of immersion, air-dried stems were coated by discontinuous regions of powdery opal-A microsphere aggregates with little structural strength which would have little effect in stabilising stems against collapse. However, following 330 days, dense opal-A films of up to several hundred microns encrusted stem surfaces. Films reached their greatest development on those surfaces which lay facing upwards during deposition and were most frequently exposed to drying conditions between eruptions. Such deposits probably formed in a manner similar to that active during rapid sinter apron accretion (Rimstidt & Cole 1983) because evaporation during exposure either encouraged precipitation of opal-A on the organic substrate or increased cementation of formerly suspended opal-A microparticles to exposed surfaces.

Three major routes of ingress of silica into plant stems appear possible: longitudinally via the rhizomes, radially across the cuticle/epidermis, and from point sources such as wounds, tears and the stomata. Experimental material was immersed whilst alive and with rhizomes intact. At least initially, geothermal fluid may have actively been taken up by the plant. However, vent fluid temperatures in excess of c. 50°C would lead rapidly to plant death. Passive transport mechanisms such as diffusion and capillary action (Jones *et al.* 1998) would then become important.

The death of stomatal cells and reduction of cell turgor should initially result in the closure of stomatal apertures and the prevention of fluid ingress. However, opal-A deposited between guard-cells of subfossil pine material (Fig. 9e) illustrate *post mortem* opening of stomata. This process most likely occurs following exposure of epidermal surfaces to drying conditions and desiccation/shrinkage of cells/tissues. Open stomata would create point source channels for the entry of fluids to intercellular spaces. Additional points of silica ingress may have been provided by epidermal tears and wounds, considered by Spicer (1991) to enhance rates of fluid entry to plant tissues and increase rates of waterlogging.

The main functions of the cuticle during the life of a plant are to provide protection against excessive water loss and to prevent leaching of inorganic and organic solutes by external fluids (e.g. Marschner 1995, p. 120). The cuticle has pores of up to 1 nm which allow evaporation of water through the cuticle (peristomatal/cuticular transpiration) and inward permeation of low molecular weight solutes (e.g. mineral elements). Fixed negative charges (from polygalacturonic acid components of the cuticle) line the pores; these enhance the permeability of the cuticle to cations, but repulse anions (Marschner 1995 p. 121). Silica occurs in geothermal solution as $Si(OH)_4$ (monosilicic acid), a neutral molecule (Fraústo da Silva & Williams 1993)

with a relative molecular mass of 96·2 (Raven 1983) and subnanometer diameter (low molecular mass silicic acids such as trisilicic acid have diameters of less than 0·265 nm or 2·65 Å; Sullivan 1986). Therefore, silica should be able to traverse pores in fresh (non-degraded) cuticle.

Increasing the temperature of epicuticular and cuticular waxes in the range 17–34°C increases rates of water and solute mobility by reducing the viscosity of amorphous waxes through which the solutes are diffusing and by decreasing the tortuosity of the solute diffusion path (Schönherr & Baur 1996, and references therein). Schreiber (2001) investigated the effect of temperature on cuticular transpiration in five species of angiosperm, finding that permeation of the cuticle by water increased significantly (by factors between 12 and 264) as temperatures increased above 30°C. Cuticular waxes (Aggarwal 2001) and alkanes (major components of cuticular waxes) reach melting points in the temperature range c. 45–75°C (e.g. Coutinho *et al*. 1995; Górecki *et al*. 2000; Paunovic & Mehrotra 2000). Water temperatures in the pool environment of this experiment are likely to have decreased epicuticular and cuticular wax viscosity dramatically, and led to the melting and separation of waxes from other organic components of the epidermal cell wall. Extracting cuticular waxes from cuticular membranes increases their permeability to water and solutes by up to three orders of magnitude (Schönherr & Baur 1996, and references therein). Melting of epicuticular waxes and liberation of cuticular waxes may represent a major mechanism leading to silica ingress in environments which experience fluid temperatures over c. 30°C. In the vent pool environment, high-temperature alkali hydrolysis might also degrade the epicuticular waxes and cuticle. The effects of alkali hydrolysis on the water-insoluble waxes may only be slight (extraction of cuticular waxes/lipids is usually effected by immersion in organic solvents; e.g. Riederer & Markstädter 1996). Wax melting/removal during the earliest stages of immersion may have stripped early opal-A microparticle/film deposition, resulting in the apparently poor surface encrustation observed following 30 days.

An additional mechanism of wax removal may involve the absorption of lipids to opal-A surfaces. Diatomites (biogenic amorphous opal-A) are used commercially as a pesticide because they adsorb lipids from the insect carapace onto opal-A surfaces and into micropores within the opal-A structure (e.g. Korunic 1997, and references therein). This leads to thinning of the protective waxes and water loss and desiccation of the insect body. Periods of exposure of stem surfaces to the atmosphere and evaporation would be required for this process to progress in the vent environment since microparticles with low moisture content are most effective at adsorbing lipids (Fields & Korunic 2000). Adsorption of lipids to opal-A surfaces may be an important process of plant degradation in evaporative environments such as sinter aprons.

Following penetration of the plant's outer tissues, transport of dissolved silica proceeds via intercellular and intracellular pathways through the remaining tissues. In life, large intercellular air spaces, such as the longitudinal lacunae of *Eleocharis*, maintain an internal pressurisation (Sorrell & Tanner 2001). Following the immersion and death of the plant, internal pressurisation would be lost as stomata lost function and fluid inflow could progress rapidly. Opal-A film deposition within the lacunae of the initial experiment indicates that silica-laden water entered and was deposited on cell walls lining the lacunae within 30 days of immersion. Sites of opal-A deposition within 30-day material indicate that, early in the silicification process, silica was transported through stems primarily via apoplastic routes (intercellular spaces and primary cell walls) and through intercellular spaces created by degradation of the middle lamella/primary wall. Transport across primary walls in the earliest stages of this process may have required that silica be transported in the monomeric state or as low-molecular-mass silica polymers. Pores in the primary cell walls (interfibrillar and intermicellar spaces), which typically have diameters of 3·5–3·8 nm (but may reach up to 5 nm) may also have been permeable to Si macromolecules of colloidal dimensions (with diameters of less than c. 5 nm). However, larger colloids may have been prevented from crossing cell walls during diffusion in a dialysis or ultra/microfiltration-like process that could lead to concentrations of nano/microspheres adhered to cell wall surfaces (Fig. 11).

Silica transport into secondarily thickened cells could progress via three routes. Longitudinal transport of fluid taken up by rhizomes within xylem elements may have persisted initially until evapotranspiration ceased. Following cessation of such mass flow, diffusion would become the primary mode of fluid/silica transport. Movement of silica would then progress via either pits and perforations in cell walls, or across cell walls themselves. Both pathways require cell degradation, the breakdown of pit-closing membranes and cell-wall waterlogging respectively, to progress before becoming active.

Epidermal cells and fibres of the peripheral sclerenchyma bundles containing lumen-lining opal-A films appear to illustrate the rapid permeation of thickened and lignified secondary cell walls, and the creation of inward-moving fronts of silicification, envisaged by Powell (1994) and Trewin (1996), within 30 days of deposition. Immersion in hot alkaline fluids directly after collection placed stems in an environment where waterlogging and hydrolytic degradation of tissue structure, particularly cells at the periphery of stems, would be promoted. Scurfield & Segnit (1984) reported that lignified cell walls, when water swollen, contained a reticulate network of micropores with diameters from c. 0·8–3·6 nm. Following waterlogging, both primary cell walls and lignified cell walls within stems would be freely permeable to dissolved silica and low-molecular-mass silicic acids which could be transported throughout stems by diffusion. The large cells of the central ground tissue and outer vascular bundle sheaths, which initially resisted silica ingress, also lack pits/perforations. Silica transport into the tissue would have to occur across the lightly lignified cell wall. The central location of the cells potentially buffered them from high water temperatures, apparently reducing rates of cell-wall degradation and silica permeation.

Silica transport to secondarily thickened cells would also occur through pits and perforations. Differences in the degree and position of pitting/perforation would alter pathways and rates of silica diffusion into cells, potentially creating microenvironments where, at least initially, silica supersaturation was retarded or levels of supersaturation kept low. Fibres of the inner bundle sheaths were pitted, with c. 15–30 submicron pits per fibre. Pitted areas would become freely permeable to silica in solution following breakdown of pit membranes. However, the cells lacked opal-A deposits after 30 days. Rates of transport into the fibre sheaths and equilibration of fluids via diffusion through the pits may have been retarded because of their position within the cylinders of imperforate parenchymatous cells of the outer sheaths. Similarly, the lack of opal-A in the metaxylem vessels, with scalariform, reticulate and helical thickenings, and relatively large perforated areas of wall, may be attributable to their position within the compact tissues of the bundle sheaths and low rates of radial fluid transport through those tissues.

The observations above illustrate that silica infiltration remains to some extent under the control of the plants organic frame during the earliest stages of the silicification process. The lignified cell walls of fibres within the vascular bundle sheath

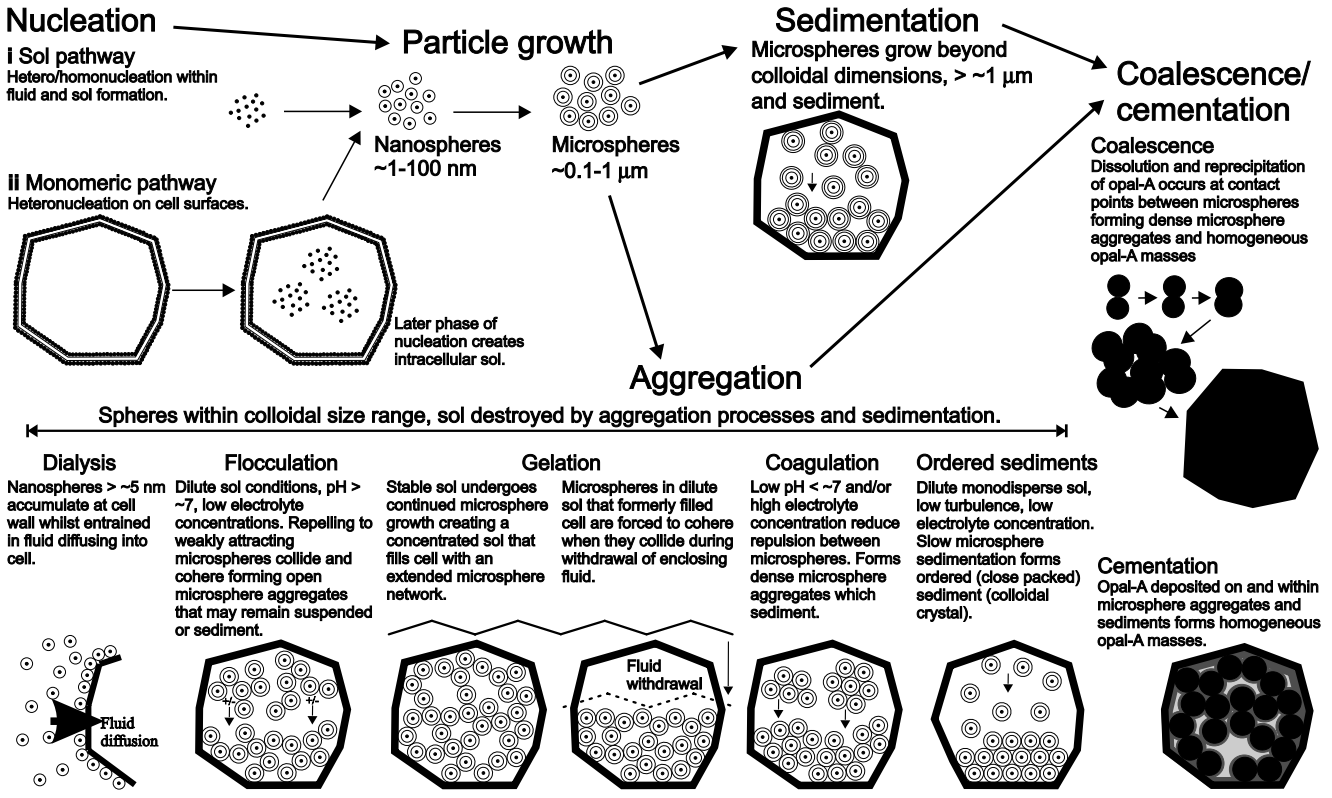


**Figure 11** Summary diagram illustrating the pathways and processes of opal-A fabric development.

and large cells of the central ground tissue strands remained impermeable to silica. This illustrates differential rates of cell wall permeation across the stem which most likely relate to the interplay between the position of tissues relative to external fluids, position relative to other tissues and cell structure/ composition.

The initial differential-response of secondarily thickened/ lignified cells to silica permeation appears to have been overcome within the duration of the 330-day experiment. Further dissolution of lignified cell wall components (to the point of fibre separation, a loss of c. 30% dry weight) is accompanied by an increase in pore diameter to c. 56 nm (Scurfield & Segnit 1984). As cell walls reached this level of degradation, the entire stem structure would be permeable to silica in solution plus potential movement of colloidal opal-A microspheres. Separation of fibres (e.g. Fig. 9a) and xylem cells (e.g. Fig. 8b, c) following 330 days indicates that this process was well advanced within stems prior to tissue stabilisation. However, lignified cells were generally permeated prior to their collapse, indicating that, even though components of their cell walls were being removed, and fibrillar and microfibrillar structures were separating, the cell walls remained resistant to collapse until stabilisation by opal-A.

## 4. Stages of silicification

### 4.1. Nucleation

Two styles of silica nucleation are possible within plant material (Fig. 11). Cell walls, cell contents and dissolved/ suspended mineral components of vent/intraorganic fluid may provide surfaces for heterogeneous nucleation (e.g. Iler 1979; Rimstidt & Cole 1983), whilst high levels of silica supersaturation may promote homogeneous nucleation of monomer to polymeric silica and colloidal opal-A nano- and microspheres (e.g. Iler 1979; Williams & Crerar 1985; Fournier *et al.* 1991; Yee *et al.* 2003).

Within intercellular regions, void-size appears to influence the style of opal-A deposition. Large intercellular spaces such as the lacunae in the central ground tissue with large expanses of cell-wall, film-like opal-A deposition and an absence of space-filling microsphere aggregates appear to represent areas within the stem where nucleation/deposition was concentrated on cell wall surfaces. It is unclear whether the earliest deposition to these surfaces was via monomeric silica deposition or aggregation/accumulation of polymeric/colloidal opal-A via electrostatic/van der Waals forces at cell-wall surfaces (e.g. Yee *et al.* 2003). Protrusions on the lacunae-facing surfaces of lacunae-lining cells (Fig. 10a) indicate that some intercellular microspheres were nucleated, perhaps on heteronuclei suspended or dissolved in intercellular fluid. Following a period of growth, microspheres became adhered to the lacunae walls. Further deposition of dense opal-A then appears to have evened out the topography created by microsphere adhesion, confirming that deposition on these surfaces, but not intercellular nucleation/microsphere growth, occurred during later influxes of silica. Deposition of opal-A on cell surfaces and other heteronuclei within these spaces appears to have kept silica supersaturation at a low level, preventing homogeneous nucleation of large numbers of opal-A nano/microspheres.

Smaller intercellular spaces created by tissue degradation (i.e. areas of the protoxylem in Fig. 8g) often exhibited a wider microsphere size distribution than sites of more restricted silica supply. The free movement of intraorganic fluid and silica diffusion through these areas, but relatively small surface area for opal-A deposition, may have allowed further opal-A nucleation events.

The smallest areas of intercellular porosity, characterised by bosses of homogeneous opal-A, (e.g. Fig. 6g), appear to illustrate that, following microsphere growth to dimensions which forced aggregation, further opal-A deposition occurred on and within the microsphere aggregate.

Nucleation of opal-A on the external surfaces of parenchymatous cells, within intercellular spaces and within cell walls,

meant that much silica transported to areas adjacent to cell walls in the initial experiment was polymerised before entering the cell. The lack of microsphere aggregates within intracellular spaces suggested that silica saturation within these areas of the stem generally remained below or at low levels of supersaturation. In the vent pool, high water and substrate temperatures may have kept the levels of silica supersaturation within stems at low levels. For instance, at a temperature of 70°C silica supersaturation is reached at c. 250 mg $kg^{-1}$, as opposed to c. 50–60 mg $kg^{-1}$ at c. 25°C. Therefore, vent fluid with c. 350 mg $kg^{-1}$ dissolved silica is supersaturated to a lower degree at high temperatures. In addition, the amount of silica available for deposition before silica concentration falls below saturation is reduced if the higher fluid temperature is maintained. At higher temperatures and whilst rates of silica diffusion into a stem are slow, opal-A deposition onto the external surfaces of cells and/or in intercellular spaces may provide sufficient surfaces for nucleation/deposition to rapidly deplete available silica to below saturation.

The presence of intracellular opal-A microspheres following 330 days indicates that, prior to the collapse of many parenchymatous cells, rates of monomer diffusion into cells were too great, and rates of deposition onto cell walls and formerly deposited opal-A too low to prevent high degrees of intracellular silica supersaturation and (most likely) homogeneous nucleation within the intracellular fluid. Nucleation resulted in the creation of an intracellular silica sol (a suspension of colloidal opal-A microspheres). A prolonged period of low vent-fluid level and exposure of the vent pool floor around the experiment most likely initiated nucleation. In these conditions, temperatures within stems would fall and levels of silica supersaturation increase. The decay products of cell walls, organelles, cytoplasm and dissolved elements may also have provided additional nucleation surfaces within intracellular fluid. Opal-A films lining the inner walls of parenchymatous cells may represent opal-A nucleation and microsphere growth within the decaying cytoplasm. However, the patchy distribution of films lining most inner cell walls appears to suggest that cytoplasm and cell membrane degradation preceded nucleation.

The large number and narrow size distribution of the microsphere populations within many parenchymatous cells indicate either spontaneous and widespread homogeneous nucleation, or the presence of large numbers of nucleation sites available as the silica concentration within cell lumina reached critical supersaturation (Everett 1994, p. 61). The same observations may also indicate that the interval of time over which this initial nano/microsphere nucleation took place was extremely short since the diversity in microsphere size within a lumen would increase as the duration of the initial nucleation event increased (Everett 1994, p. 61, fig. 4.3). Here it is envisaged that silica concentration within the cell lumen rose slowly to the level of critical supersaturation. At this point, formation of nuclei began. As nucleation progressed, silica concentration began to fall because monomer was being depleted from the essentially closed environment of the cell. Nucleation then ceased as silica concentration fell to below the level of supersaturation once more. Differences in nucleus size would be minimal. Following this initial nucleation event, growth of existing nuclei would be favoured over further nucleation.

The narrow microsphere size distribution observed across entire areas of tissue confirms that the nucleation process within parenchymatous cells was affected by widespread and perhaps large-scale changes in the physicochemical character of the intraorganic environment. These were most likely a result of changes in geothermal activity, but may also have been influenced by organic processes. The following example is provided as an illustration of a possible sequence of events that would allow widespread and rapid nucleation.

A prolonged period of high vent-fluid level immersed the stem in high-temperature vent-fluid. During immersion, silica diffused through the cortical tissue and through the cell walls. However, the elevated water temperature of the vent pool and opal-A deposition on and within cell walls kept intracellular silica concentrations below supersaturation, thereby preventing homogeneous nucleation. The period of high water levels came to an abrupt end and the stem became emergent. Temperature within the stem dropped, forcing silica within the lumina to become supersaturated rapidly. Nucleation progressed rapidly, either until the intracellular silica concentration was depleted enough to prevent further nucleation or until equilibrium with the new intracellular temperature was reached. Subsequent immersion events would then promote microsphere growth as discussed below (see Section 4.2). Rapid supersaturation and nucleation may also have been influenced or caused by fluctuations in vent-fluid temperature or pH, and also changes in intracellular pH.

The relatively low number of opal-A microspheres observed within many vascular and sclerenchyma cells may reflect a paucity of nucleation sites within dead/lignified cells relative to parenchyma. Remnants of cell contents are not available as sites of nucleation in lignified cells. Nucleation sites of inorganic origin may have provided the only available surfaces for heterogeneous nucleation. Cellulose cell walls were observed to provide excellent nucleation surfaces in the initial experiment. The slower rate of degradation expected from lignified cells and the polymer's hydrophobic nature may suggest that organic nucleation surfaces were absent or unavailable from intracellular spaces within lignified cells. The delayed availability of nucleation sites may in part be responsible for the limited extent of, and apparently staggered start to, opal-A deposition within many sclerenchyma and xylem cells. Alternatively, the rate of silica supply, for instance across the pitted secondary wall of fibres within the inner vascular bundle sheath, may have been relatively slow and the level of silica supersaturation low. In these circumstances, nucleation sites on cell-wall surfaces may have provided sufficient areas of opal-A deposition to prevent either hetero- or homogeneous nucleation of microspheres within the intracellular fluid.

### 4.2. Polymerisation, nanosphere/microsphere growth and sol formation

Brownian motion, fluid turbulence, pH between 7 and 10, and low salt concentrations all promote the growth of colloidal opal-A microspheres by preventing aggregation (e.g. Bergna 1994). The growth of isolate opal-A microspheres to c. 800–900 nm during the present experiment indicates that one or more of these processes was active within intracellular sites. The maintenance of intracellular sols appears likely to be influenced most strongly by local pH and salt concentrations, since Brownian motion would be experienced by microspheres irrespective of the intraorganic environment, and intraorganic turbulence was likely to be minimal. The maintenance of a high intracellular pH (greater than 7) and the exclusion of salts (or maintenance of salt concentrations below a critical coagulation concentration) are prerequisite to continued microsphere growth (e.g. Iler 1979; Williams & Crerar 1985; Bergna 1994).

The shell structure of acid-etched microspheres may illustrate cyclic variation in rates of opal-A deposition to microsphere surfaces. The shell layers and voids illustrate subtle differences in the solubility of opal-A forming each layer, and most likely represent differential responses of alternating wet

and dry (Jones & Renaut 2004), or open and dense layers of opal-A to the acid etching process. Two mechanisms of shell formation appear possible. The cyclic fluctuations of physical and chemical environment inherent to hot spring vent pools may have triggered alternating periods of high silica supersaturation, rapid opal-A polymerisation and wet/open laminae deposition (most likely during periods of vent pool cooling or drying), and low silica supersaturation, slower deposition and dry/dense laminae deposition (during periods of immersion and high vent fluid temperature). Alternatively, in more stable physical conditions (e.g. if temperature remained relatively constant following initiation of deposition), laminae could represent opal-A precipitation-monomer depletion events. Here, opal-A deposition at high degrees of supersaturation would be rapid, taking a polymeric pathway resulting in wet/open laminae. This rapid polymerisation would deplete available monomer, the level of supersaturation would drop and the rate of opal-A deposition would fall, creating dry/dense laminae. Reduction in levels of saturation could potentially switch opal-A deposition from a polymeric to a monomeric pathway (e.g. Iler 1979; Fournier 1985).

The predominance of microspheres near the upper limit of colloidal size indicates that, following intracellular nucleation, the surfaces of microspheres and earlier cell-wall linings became the preferred sites for subsequent opal-A deposition. The continued growth of early formed intracellular microspheres and maintenance of a narrow size distribution requires that the rate of silica supply to intracellular spaces remained lower than the rate of microsphere growth (Everett 1994, p. 61). An excess of monomer within a cell lumen would cause periods of fresh nucleation. Therefore, it appears that silica supply to the intracellular regions of parenchymatous cells remained slow relative to the growth of microspheres. Silica supply may have been regulated by the continued presence of relatively intact cell walls, as described above. Opal-A deposition on and within cell walls may also have restricted diffusion within the progressively more indurated stem.

The relatively large size, narrow size distribution and generally low degree of coalescence of intracellular microspheres indicate that the period of microsphere growth continued within cells which retained intracellular fluids and maintained sol conditions. Differing degrees of sol concentration are indicated within cells (Fig. 11). Ordered microsphere sediments (Fig. 10e, f) indicate very dilute sol conditions, whilst cells completely filled by microsphere aggregates (e.g. Fig. 7c) indicate highly concentrated sols where the particle fraction almost completely filled the cell lumen. Disordered microsphere sediments (e.g. Fig. 9d) illustrate the presence of sols dilute enough to allow microspheres to settle from suspension, but concentrated enough to promote microsphere collisions and aggregation (flocculation/coagulation). Microspheres adhered to the upper regions of these latter cells indicate that fluid also completely filled these cell lumen during the period when microspheres were approaching the upper limit of colloidal stability (Fig. 9d). However, whilst in the sol, some microspheres came into contact with the surfaces of wall-lining opal-A (or cell walls themselves), and the repulsive force between the two surfaces was sufficiently small to permit cohesion of the microspheres and surface.

### 4.3. Destruction of sols and microsphere deposition

Open networks of microspheres which partially to completely filled intracellular spaces with open, poorly coalesced microsphere aggregates appear to represent intracellular sols destroyed by coagulation/flocculation or gelation (e.g. Figs 6c, e, 9c). As discussed above, these cells were apparently filled with a relatively concentrated sol. Within cells filled completely with microsphere aggregates, fluid was obviously initially present throughout the intracellular/interparticle space to allow filling of lumina. The creation of a highly concentrated sol within the confined space of these cell lumina was probably brought about by continued microsphere growth which promoted gelation because of the increased likelihood of microsphere collisions. Additionally, the progressive degradation of cellular material may have created a localised fall in pH that would reduce repulsion between microspheres, and favour collision and adhesion. Gelation was particularly apparent in parenchymatous cells which contained microsphere populations well below the upper size limit of colloidal stability and open, three-dimensional microsphere networks with very few areas of increased microsphere density (e.g. Fig. 6c, e).

Microsphere growth within narrow lumina (e.g. within fibres and narrow metaxylem vessels) would create concentrated sol conditions, comparable with those above, more rapidly than in large parenchymatous cells. In these environments, even relatively late permeation of cell walls, or breach of pits and perforations could rapidly lead to the creation of cell-lumen-filling microsphere networks (e.g. the occasional metaxylem cells of Fig. 8a, b, g). These sites appear comparable with small intercellular sites filled with dense homogeneous opal-A because, once microsphere networks fill the cell lumen, further opal-A is deposited on and within the network, thereby creating homogeneous opal-A masses (e.g. xylem vessels in Fig. 8e).

Microsphere growth in a sol may also be halted by sedimentation, either as microspheres collide and aggregate (flocculate/coagulate), or as they become too large to prevent sedimentation (e.g. Bergna 1994). Evidence for sedimentation was common within intercellular and intracellular spaces within stems. Intercellular microsphere aggregates of limited extent accumulated at the bases of the large central-ground-tissue lacunae (e.g. upper central lacuna of Fig. 6b) and within smaller intercellular spaces created by organic degradation (e.g. the degraded region of protoxylem in Fig. 9d). Microsphere sediments within parenchymatous cells of the central ground tissue formed obvious way up structures (i.e. Fig. 7a, c).

Microspheres within these sites commonly approached the c. 1 μm upper size limit of colloidal stability. As microsphere size increased to these dimensions, the forces which maintained interparticle repulsion, and therefore, colloidal stability would be overcome. At this point, isolated microspheres could settle from suspension. Microsphere aggregation phenomena (flocculation and coagulation) within intraorganic fluid could also cause smaller microspheres to group together and settle to the base of cells (e.g. Bergna 1994). The relatively dense nature of microsphere sediments at the bases of cells (e.g. Fig. 7c, d) may suggest that coagulation, the formation of relatively dense clumps of microspheres, dominated sedimentation in these cells. However, sediments formed of isolate microspheres or more open floc-like particle aggregates may develop comparable fabrics following further opal-A deposition (cementation) or a period of microsphere coalescence. Here it is considered that most microspheres were deposited as isolated entities as their size reached c. 750–900 nm, and that opal-A deposition and coalescence occurred by mechanisms described below.

An alternative mechanism for the deposition of microspheres at the 'base' of cells and intracellular voids involves the withdrawal of the suspending medium (Fig. 11). Evidence discussed above suggests that many cells were full of fluid immediately prior to microsphere deposition. Draw-down of this fluid, for instance during a period of low vent-fluid level, would concentrate microspheres remaining within the cell

lumen or intercellular space. This would create a more concentrated sol where microsphere/microsphere collisions and interparticle cohesion could be promoted. Gelation by this method would create open aggregates, as discussed above.

Close-packed and extremely well-ordered microsphere sediments developed within the intracellular spaces of the outer cortex of *E. flavescens* stems during the 330-day experiment (Fig. 10e, f). Microsphere size variation within the sediment was very narrow and approached a unimodal distribution. The formation of this sediment required quite specific conditions which illustrate the type of chemical and physical conditions which occurred within intraorganic sites during the latter stages of opal-A deposition. Ordered opal-A microsphere sediments produce the play of colour associated with gem opal (Darragh *et al*. 1976). The creation of such colloidal crystals was investigated experimentally by Davis *et al*. (1989, 1991). Conditions which were experienced during the creation of this sediment were likely to be identical to those in the creation of gem opal and experimentally prepared colloidal crystals. The process requires the creation of monodisperse sols, as described above. Observation of the disorder-to-order transition of settling monodisperse colloidal opal-A microspheres (Davis *et al*. 1989, 1991) shows that large particle size increases sedimentation rate beyond the rate of crystalline ordering. Experimental observation also suggests that low pre-settlement microsphere volume fractions favour settlement to ordered sediments, whilst high microsphere volume fractions produce amorphous sediments (Davis *et al*. 1989, 1991). This indicates that dilute intracellular sol conditions and slow sedimentation occurred within the tissue. Conditions within the stem were also relatively stable physically and chemically. The formation of gem opal is considered to require the slow evaporation of a relatively pure neutral to alkaline silica solution, with low salt concentration and an absence of natural coagulants, such as oxyhydroxides or clays (Williams & Crerar 1985). Such conditions occurred in the intracellular spaces of this material at the time of microsphere deposition.

The absence of ordered sediments from other tissues observed in this material indicate deviation from these physicochemical conditions. Because microspheres in ordered and disordered sediments are of comparable size, settling-rate-related phenomena appear unlikely to have caused differences in sediment order. This suggests that deviation of salt or coagulant concentration, and/or local pH created disorder in other tissues. Local differences in pH, resulting from stem degradation, appear to provide a simple mechanism that would cause microsphere aggregation and prevent colloidal crystal formation. The relatively high concentration of salts in vent fluid would also promote aggregation.

### 4.4. Microsphere coalescence/cementation

Many intracellular sediments were characterised by an increasing degree of microsphere coalescence and/or infilling (cementation) from top to bottom (e.g. Fig. 7c, d). Two mechanisms which may have operated at various times appear likely to have created this fabric (Fig. 11). If intracellular fluid levels were fluctuating within the microsphere sediment as vent-fluid level fluctuated, microspheres at the base of the sediment pile would be in contact with opal-A-depositing fluids more often than those at the upper margin. Cementation by the addition of further opal-A would preferentially fill porosity at the base of cells. The juxtaposition of open microsphere aggregates and dense, homogeneous opal-A (indicated in Fig. 7a–c) suggest that, if this were the case, individual cells at comparable positions relative to vent-fluid level acted as isolate microenvironments. Another alternative mechanism of creating homogeneous opal-A, microsphere coalescence is involved in sinter accretion (Rimstidt & Cole 1983; Williams & Crerar 1985). Coalescence progresses as opal-A dissolves and reprecipitates at the contact points of microspheres. The increased coalescence observed towards the base of sediments in the present study may reflect minor differences in pressure at the contact points between adjacent microspheres. Pressure experienced at contact points at the base of the sediment would be greater than that experienced at the top, resulting in a greater rate or extent of microsphere dissolution/reprecipitation at the base of sediments.

## 5. Comparison with Rhynie chert plants

The high-temperature vent pool setting of this experiment differs from the lower temperature pool margin/sinter apron environments envisaged for the growth and preservation of the Rhynie plants. However, the experimental silicification of modern plant material documented here replicated the exceptional three-dimensional preservation characteristic of many Rhynie chert plant fossils. Parenchymatous cells, which would be rapidly destroyed in most terrestrial settings, appeared, as in many Rhynie plants, to have a taphonomic potential equal to normally more resistant secondarily thickened/lignified cells. Further similarities between experimental and Rhynie material include geopetal fabrics/silica sediments filling the bases of cells/voids, inward moving fronts of silicification and the development of stem-encrusting silica films (e.g. Powell 1994; Trewin 1996).

High temperature, high pH and waterlogging may all have acted to promote cellular preservation in the vent pool by preventing the activities of plant degrading microbes. Of these factors, the present authors consider that waterlogging is likely to have been of primary importance in increasing the preservation potential of parenchymatous cells in the cooler environments of Rhynie since desiccation of such thin-walled cells prior to stabilisation with silica would result in rapid tissue collapse. Additionally, as hot spring fluid temperature drops from eruption temperature to ambient, the degree of silica supersaturation rises while, at the same time, degassing of $CO_2$ causes an increase of pH and evaporation increases salinity/alkalinity. These processes may have positively affected the preservation potential of the Rhynie plants. Increased silica supersaturation would increase the rate and extent of silica deposition onto and within plants, whilst increased pH and salinity/alkalinity would further inhibit the activity of bacteria and fungi.

The low stomatal densities and often reduced rhizomes of the Rhynie plants imply that dissolved silica transport primarily progressed radially across the cuticle and epidermis. However, water temperatures in the distal hot spring environments considered to be common sites of plant preservation at Rhynie were probably lower than those experienced by experimental material of the present study. Therefore, complete melting and stripping of cuticular waxes appears unlikely to have occurred at Rhynie. Upper reported temperatures (c. 30–35 °C) of emergent aquatic plant growth in modern, hot-spring-influenced wetlands (e.g. Channing 2001, 2003) fall at or below the temperature (30 °C) at which Schreiber (2001) observed significant increases in permeances of water across cuticles. The disruption of cuticular function is amply displayed in Rhynie plants by the inward moving fronts of silicification described by Powell (1994) and Trewin (1996). At Rhynie, temperatures in the environment of silicification and cuticular permeability were clearly sufficient to allow radial ingress of dissolved silica.

Because hot-spring-influenced wetlands can provide both constantly wet conditions and relatively high water temperatures, which respectively promote plant waterlogging and

dissolved silica permeation of axes, they appear favourable environments for the exceptional preservation exhibited by many Rhynie plants (e.g. Channing 2001, 2003; Trewin *et al.* 2003; Trewin & Wilson 2004).

## 6. Conclusions

Plant material introduced into silica-supersaturated fluids of the vent pool of Medusa Geyser showed evidence of incipient silicification within 30 days of immersion. Inter- and intracellular silicification of epidermal cells and peripheral bundles of fibres suggest that elevated temperature rapidly melts and/or strips epicuticular and cuticular waxes and promotes waterlogging of secondarily thickened and lignified cell walls. This radial transport of silica in solution sets up inward-moving fronts of silicification. At the same time, loss of stomatal function leads to the loss of stem internal pressurisation, and this allows fluid to fill internal air spaces within stems. Silica is transported to intercellular sites and is deposited on external cell surfaces and within primary cell walls. Silica deposition takes the form of relatively smooth silica films which may represent either widespread heterogeneous nucleation of monomeric silica directly onto cell surfaces or accumulations of homogeneously nucleated polymeric silica/colloidal opal-A nanospheres adhered or aggregated at cell surfaces. Unambiguous colloidal nano/microspheres nucleate, polymerise and grow to c. 1–200 nm diameters within smaller microenvironments, particularly at the intercellular junctions of groups of cells. Growth and aggregation creates dense, structurally robust and brittle space-filling opal-A masses which as they develop, would begin to stabilise tissues structurally against collapse, and replicate cell and tissue morphology by cast and mould preservation. Differential permeation of tissues by dissolved silica in this earliest period of the silicification process illustrates that tissue and cell morphology, structure, biochemical composition, and location relative to external high temperature fluids and other tissues strongly influence rates of silica permeation, and creates intraorganic microenvironments.

The physical and biochemical attributes which impart tissues/cells with a resistance to silica ingress also appear to impart a structural and chemical stability in the vent environment that prevents excessive degradation prior to the onset of silicification. This is evidenced by material collected following 330 days immersion that illustrates an eventual reduction in the influence of the organic frame of the plant on fluid and silica infiltration, and the permeation of all tissues and cells by silica. Formerly incipient opal-A films increase in thickness to 500–1000 nm, creating structurally robust layers which line practically all observed organic surfaces. Opal-A microsphere aggregates which dominate intraorganic fabrics document the nucleation, polymerisation, growth and destruction of essentially monodisperse inter- and intracellular opal-A sols. The unimodal size distribution of microspheres within single cells appears to suggest a single, rapid and short-lived nucleation event. Growth of microspheres was via alternating/cyclic phases of dense/dry and open/wet opal-A accretion which demonstrate alternating periods of high and low silica supersaturation, potentially caused by variation of the physicochemical environment within specimens (i.e. cycles of cooling and heating), or a stable environment affected by periods of opal-A precipitation and depletion of monomer. Sol conditions within many plant cells remained stable (suggesting high intraorganic pH and low salt concentrations) long enough for microspheres to reach dimensions approaching the upper limit of colloidal stability and form ordered gem-opal-like sediments. In other cells, sol conditions were destroyed by gelation as microsphere growth created an ever more concentrated sol and forced microsphere–microsphere collisions. In yet other cells, microspheres in dilute sols were aggregated by flocculation/coagulation, or individually grew beyond colloidal dimensions and settled to the bases of cells, forming sediments. Similar fabrics may also have formed during periods of drying and withdrawal of fluid from intraorganic environments. Following sol destruction, microsphere aggregates often underwent a subsequent period of coalescence at contact points and/or cementation that, in extreme cases, locally completely occluded porosity and created internally homogeneous masses of opal-A.

The extreme heterogeneity of opal-A fabrics displayed by the material described in the present study emphasises the dynamic physical and chemical conditions prevailing in hot spring environments, and the heterogeneity of the intra-plant environment (in life and death) as a frame through which silicifying fluids flow and on which opal-A is deposited.

## 7. Acknowledgements

The authors would like to thank the US National Park Service for permitting fieldwork and collecting in Yellowstone National Park. The staff of the Yellowstone Centre for Resources are thanked for logistic and technical assistance. Bill Wise, Smokey Sturtevant and the interpretive staff of Norris Geyser Basin are thanked for their assistance in accessing geothermal areas. We gratefully acknowledge Peter Fisher, Tony Oldroyd, Colin Lewis and Sarah Goldsmith for assistance with analytical techniques. Carolyn Davies, Lyall Anderson and Nigel Trewin are thanked for assistance during fieldwork. This study was conducted whilst AC was the recipient of NERC Research Studentship GT4 97 ES.

## 8. References

Aggarwal, P. 2001. Phase transition of apple cuticles: a DSC study. *Thermochimica Acta* **367–368**, 9–13.

Bergna, H. E. 1994. Colloid chemistry of silica: an overview. *In* Bergna, H. E. (ed.) *The Colloid Chemistry of Silica*. *Advances in Chemistry Series* **234**, 1–47. Washington, DC: American Chemical Society.

Coutinho, J. A. P., Anderson, S. I. & Stenby, E. H. 1995. Evaluation of activity coefficient models in prediction of alkane solid-liquid equilibria. *Fluid Phase Equilibria* **103**, 23–39.

Channing, A. 2001. *Processes and environments of vascular plant silicification*. Unpublished Ph.D. thesis, Cardiff University.

Channing, A. 2003. The Rhynie Chert early land plants: palaeoecophysiological and taphonomic analogues. *Transactions of the Institutions of Mining and Metallurgy: Section B, Applied Earth Science* **112**, B170–1.

Darragh, P. J., Gaskin, A. J. & Sanders, J. V. 1976. Opals. *Scientific American* **234**, 82–95.

Davis, K. E., Russel, W. B. & Glantschnig, W. J. 1989. Disorder-to-order transition in settling suspensions of colloidal silica: x-ray measurements. *Science* **245**, 507–10.

Davis, K. E., Russel, W. B. & Glantschnig, W. J. 1991. Settling suspensions of colloidal silica: observations and x-ray measurements. *Journal of the Chemical Society: Faraday Transactions* **87**, 411–24.

Everett, D. H. 1994. *Basic Principles of Colloid Science*. London: Royal Society of Chemistry Paperbacks.

Fields, P. & Korunic, Z. 2000. The effect of grain moisture content and temperature on the efficacy of diatomaceous earths from different geographical locations against stored-product beetles. *Journal of Stored Products Research* **36**, 1–13.

Fournier, R. O. 1985. The behaviour of silica in hydrothermal solutions. *In* Berger, B. R. & Bethke, P. M. (eds) *Geology and Geochemistry of Epithermal Systems. Society of Economic Geologists*. *Reviews in Economic Geology* **2**, 45–61. Littleton, Colorado: Society of Economic Geologists.

Fournier, R. O., Thompson, J. M., Cunningham, C. G. & Hutchinson, R. A. 1991. Conditions leading to a recent small hydrothermal explosion at Yellowstone National Park. *Geological Society of America Bulletin* **103**, 1114–20.

Fraústo da Silva, J. J. R. & Williams, R. J. P. 1993. *The Biological Chemistry of the Elements: the Inorganic Chemistry of Life*. Oxford: Clarenden Press.

Górecki, T., Srivastava, S. P., Tiwari, G. B., Górecki, C. & Zurawska, A. 2000. Phase transitions in some *n*-alkanes and petroleum waxes – investigation by photoacoustic and exoelectron emission techniques. *Thermochimica Acta* **345**, 25–30.

Herdianita, N. R., Browne, P. R. L., Rodgers, K. A. & Campbell, K. A. 2000. Mineralogical and textural changes accompanying ageing of silica sinter. *Mineralium Deposita* **35**, 48–62.

Iler, R. K. 1979. *The Chemistry of Silica: Solubility, Polymerisation, Colloid and Surface Properties and Biochemistry*. Chichester: John Wiley & Sons.

Jones, B. & Renaut, R. W. 2004. Water content of opal-A: implications for the origin of laminae in geyserite and sinter. *Journal of Sedimentary Research* **74**, 117–28.

Jones, B., Renaut, R. W., Rosen, M. R. & Klyen, L. 1998. Primary siliceous rhizoliths from Loop Road hot springs, North Island, New Zealand. *Journal of Sedimentary Research* **68**, 115–23.

Kharaka, Y. K., Sorey, M. L. & Thordsen, J. J. 2000. Large-scale hydrothermal fluid discharges in the Norris-Mammoth corridor, Yellowstone National Park, USA. *Journal of Geochemical Exploration* **69–70**, 201–5.

Korunic, Z. 1997. Diatomaceous earths, a group of natural insecticides. *Journal of Stored Products Research* **34** (2, 3), 87–97.

Leo, R. F. & Barghoorn, E. S. 1976. Silicification of wood. *Botanical Museum Leaflets, Harvard* **25** (1), 1–47.

Lynne, B. Y. & Campbell, K. A. 2003. Diagenetic transformations (opal-A to quartz) of low- and mid-temperature microbial textures in siliceous hot-spring deposits, Taupo Volcanic Zone, New Zealand. *Canadian Journal of Earth Sciences* **40**, 1679–96.

Marschner, H. 1995. *Mineral Nutrition of Higher Plants*, 2nd edn. London: Academic Press.

Paunovic, I. & Mehrotra, A. K. 2000. Liquid-solid phase transformation of $C_{16}H_{34}$, $C_{28}H_{58}$ and $C_{41}H_{84}$ and their binary and ternary mixtures. *Thermochimica Acta* **356**, 27–38.

Powell, C. L. 1994. *The palaeoenvironments of the Rhynie cherts*. Unpublished Ph.D. thesis, University of Aberdeen.

Powell, C. L., Trewin, N. H. & Edwards, D. 2000. Palaeoecology and plant succession in a borehole through the Rhynie cherts, Lower Old Red Sandstone, Scotland. *In* Friend, P. F. & Williams, B. P. J. (eds) *New Perspectives on the Old Red Sandstone*. *Geological Society, London, Special Publication* **180**, 439–57.

Raven, J. A. 1983. The transport and function of silicon in plants. *Biological Reviews* **58**, 179–207.

Riederer, M. & Markstädter, C. 1996. Cuticular waxes: a critical assessment of current knowledge. *In* Kerstiens, G. (ed.) *Plant Cuticles: An Integrated Functional Approach*, 189–200. Oxford: BIOS Scientific Publishers.

Rimstidt, J. D. & Cole, D. R. 1983. Geothermal mineralisation 1: The mechanism of formation of the Beowawe, Nevada, siliceous sinter deposit. *American Journal of Science* **283**, 861–75.

Rodgers, K. A., Browne, P. R. L., Buddle, T., Greatrex, R. A., Hampton, W. A., Pastars, D. & Smith, B. Y. 2003. Minerals and microbes among the hot springs of New Zealand. *Mineralogical Society Bulletin* **134**, 3–8.

Schönherr, J. & Baur, P. 1996. Effects of temperature, surfactants and other adjuvants on rates of uptake of organic compounds. *In* Kerstiens, G. (ed.) *Plant Cuticles: An Integrated Functional Approach*, 135–55. Oxford: BIOS Scientific Publishers.

Schreiber, L. 2001. Effect of temperature on cuticular transpiration of isolated cuticular membranes and leaf discs. *Journal of Experimental Botany* **52**, 1893–900.

Scurfield, G. & Segnit, E. R. 1984. Petrification of wood by silica minerals. *Sedimentary Geology* **39**, 149–67.

Sorrel, B. K. & Tanner, C. C. 2001. Convective gas flow and internal aeration in *Eleocharis sphacelata* in relation to water depth. *Journal of Ecology* **88**, 778–89.

Spicer, R. A. 1991. Plant taphonomic processes. *In* Allison, P. A. & Briggs, D. E. G. (eds) *Taphonomy: Releasing the Data Locked in the Fossil Record*. Topics in Geobiology **9**, 72–113. New York, NY: Plenum Press.

Sullivan, C. W. 1986. Silicification by diatoms. *In* Evered, D. & O'Connor, M. (eds) *Silicon Biochemistry, Ciba Foundation Symposium* **121**, 90–107. Chichester: John Wiley & Sons.

Trewin, N. H. 1996. The Rhynie Cherts: an early Devonian ecosystem preserved by hydrothermal activity. *In* Bock, G. R. & Goode, J. (eds) *The Evolution of Hydrothermal Ecosystems on Earth (and Mars?)*. *Ciba Foundation Symposium* **202**, 131–49. Chichester: John Wiley & Sons.

Trewin, N. H., Fayers, S. R. & Kelman, R. 2003. Subaqueous silicification of the contents of small ponds in an Early Devonian hot spring complex, Rhynie, Scotland. *Canadian Journal of Earth Sciences* **40**, 1697–712.

Trewin, N. H. & Wilson, E. 2004. Correlation of the Early Devonian Rhynie chert beds between three boreholes at Rhynie, Aberdeenshire. *Scottish Journal of Geology* **40**, 73–81.

Williams, L. A. & Crerar, D. A. 1985. Silica diagenesis, II. General mechanisms. *Journal of Sedimentary Petrology* **55** (3), 312–21.

Yee, N., Phoenix, V. R., Konhauser, K. O., Benning, L. G. & Ferris, G. 2003. The effect of cyanobacteria on silica precipitation at neutral pH: implications for bacterial silicification in geothermal hot springs. *Chemical Geology* **199**, 83–90.

ALAN CHANNING and DIANNE EDWARDS, School of Earth, Ocean and Planetary Sciences, Cardiff University, Cardiff CF10 3YE, UK.

MS received 12 December 2003. Accepted for publication 10 June 2004.